

## A multiple-interaction model for the event structure in hadron collisions

Torbjörn Sjöstrand and Maria van Zijl

*Department of Theoretical Physics, University of Lund, Sölvegatan 14A, S-223 62 Lund, Sweden*

(Received 20 April 1987)

A detailed model for hadronic events is presented, with particular emphasis put on the event structure at low transverse momenta, i.e., “beam jets” and “minijets.” Specifically, we argue that hadronic events contain a varying number of semihard parton-parton interactions, with an average interaction rate given by perturbative QCD, and the variation between different events given by Poissonian statistics for each impact parameter separately. Comparisons with data are presented for a number of properties, such as multiplicity distributions, forward-backward correlations, minijet phenomenology, and the “pedestal effect.” Also, predictions for the behavior at higher energies are included.

### I. INTRODUCTION

In current hadron colliders the interaction between two incoming hadrons typically results in the production of 10–100 outgoing particles. We have every reason to believe that this process is described by the standard model for strong and electroweak phenomena. Unfortunately, a correct quantum-mechanical treatment does not seem to be within reach, both because of the sheer number of particles involved and because of the limited understanding of nonperturbative QCD. We are therefore in an upside-down situation where the rare processes, such as  $W/Z$  or high- $p_T$  jet production, are the easiest to understand: since they involve large momentum transfers, they are also amenable to perturbative analysis. Typical minimum-bias events, which appear with large cross sections, cannot be treated in this way.

The best that can be done at present is to try to develop simplified models. In order to account for the phenomenology already known, these models still have to be of a considerable complexity, as we shall see. In general terms, the components needed include the generation of a hard interaction by a convolution of (i) hard-scattering matrix elements and (ii) structure functions, the addition of (iii) initial-state and (iv) final-state radiation, the inclusion of (v) beam jets, and, finally, (vi) the fragmentation of partons into hadrons and the subsequent decay of unstable hadrons. Among these subjects, the structure of beam jets is certainly the least well understood.

The objective of this paper is to develop one particular scenario for strong-interaction physics at hadron colliders (elastic and diffractive events excepted). Our basic philosophy will be as follows.<sup>1,2</sup> The total rate of parton-parton interactions, as a function of the transverse-momentum scale  $p_T$ , is assumed to be given by perturbative QCD. This is certainly true for reasonably large  $p_T$  values, but in this paper we shall also extend the perturbative parton-parton scattering framework into the low- $p_T$  region. A regularization of the divergence in the cross section for  $p_T \rightarrow 0$  has to be introduced, however, which will provide us with one of the main free parameters of the model. Since each incoming

hadron is a composite object, consisting of many partons, the possibility of several parton pairs interacting when two hadrons collide should exist. It is not unreasonable to assume that the different pairwise interactions take place essentially independently of each other, and that therefore the number of interactions in a collision is given by a Poissonian distribution. Furthermore, hadrons are not only composite but also extended objects, meaning that collisions range from very central to rather peripheral ones. Reasonably, the average number of interactions should be larger in the former than in the latter case. Whereas the assumption of a Poissonian distribution should hold for each impact parameter separately, the distribution in number of interactions should be widened by the spread of impact parameters. The amount of widening will depend on the assumed matter distribution inside the colliding hadrons. Different possibilities will be compared.

The proposed route is not an easy one. It leads to a fairly complex scenario, which may make the resulting model look unattractive. However, the world of hadron physics *is* complicated, and if we err, it is most likely in being too unsophisticated. The experience gained with the model, in failures as well as successes, could be used as a guideline in the evolution of yet more detailed models.

The complexity of the model excludes the possibility of obtaining significant information by analytical techniques. Rather, the model has been implemented within the framework of the Lund Monte Carlo programs, using PYTHIA version 4.8 (Ref. 3) for points (i), (ii), (iii), and (v) above, and JETSET version 6.3 (Ref. 4) for (iv) and (vi). These programs are publicly available and can be used, e.g., to study implications for a given detector setup.

To the best of our knowledge, a scenario such as that outlined above has not been studied before. Yet, none of the individual ideas is new. A number of authors have studied the probability of having two hard interactions in an event,<sup>5–7</sup> in particular, for the production of (three or) four high- $p_T$  jets. Within the framework of dual topological unitarization (DTU),<sup>8–11</sup> the variation in the number of cut Pomerons corresponds to our variation in the number of semihard interactions. The difference is

that DTU is a nonperturbative approach, which describes the longitudinal structure of particle production. Transverse degrees of freedom can be added,<sup>10</sup> but this is not an integral part of the framework. Put drastically, our approach is an attempt to extend a perturbative, high- $p_T$  picture down into the low- $p_T$  region, whereas the DTU approach provides a low- $p_T$  model that could be extended to higher  $p_T$  values. Also the effects of varying impact parameters have been studied with respect to multiplicity distributions and forward-backward correlations,<sup>12</sup> and with respect to the increase in total cross section and the “blackening” of the proton with increasing energy.<sup>13</sup> No detailed studies have been done within the framework of multiple parton interactions, however.

The idea of multiple interactions has gained experimental support by the recent Axial Field Spectrometer (AFS) study of four-jet events.<sup>14</sup> The kinematics of these events indicates that, while some of them can be attributed to a single hard scattering with associated bremsstrahlung, a fair fraction contains two hard interactions. While no direct comparisons are made with the AFS signal, a few general comments are given in Sec. VI B.

The outline of the paper is as follows. In Sec. II the general formalism of multiple interactions is outlined, without the complication of variable impact parameters. The resulting model, as well as models without any multiple interactions at all, are compared with data in Sec. III, and some areas of discrepancy are noted. Part of the material in these two sections is taken from Ref. 1. A variable-impact-parameter picture of hadronic interactions is introduced in Sec. IV, together with necessary modifications of the multiple-interaction formalism. The phenomenology of the resulting model is covered in Secs. V and VI, in the former for multiplicity distributions and in the latter for jet properties. A summary and outlook is given in Sec. VII.

## II. THE IMPACT-PARAMETER-INDEPENDENT MODEL

### A. The QCD jet cross section

The natural starting point for our deliberations is provided by the perturbative QCD cross section for parton-parton interactions

$$\sigma = \sum_{i,j,k} \int \int \int dx_1 dx_2 d\hat{t} \hat{\sigma}^k(\hat{s}, \hat{t}, \hat{u}) \times f_i^1(x_1, Q^2) f_j^2(x_2, Q^2). \quad (1)$$

Here  $\hat{\sigma}_{ij}^k$  is the hard-scattering cross section for the  $k$ th subprocess possible between incoming partons  $i$  and  $j$ . The structure functions  $f_i^a(x, Q^2)$  give the probability for finding a parton  $i$  carrying a fraction  $x$  of the energy (and longitudinal momentum) of the incoming hadron  $a$ , if the hadron is probed at a scale  $Q^2$ . For massless partons, the three Mandelstam variables are related by  $\hat{s} + \hat{t} + \hat{u} = 0$ , and  $\hat{s} = x_1 x_2 s$ . While the  $\hat{\sigma}$  are calculable in perturbative QCD (see, e.g., Ref. 15), the structure functions are not. In the following we have chosen to use the Eichten-Hinchliffe-Lane-Quigg (EHLQ) set 1,<sup>15</sup> with  $\Lambda = 0.2$  GeV. The  $Q^2$  scale, which is also ambiguous, has been set to

$$Q^2 = p_T^2 = \frac{\hat{t} \hat{u}}{\hat{s}}. \quad (2)$$

In the study of absolute jet cross sections, it will become necessary to introduce a  $K$  factor to account for higher-order corrections to the lowest-order  $\hat{\sigma}_{ij}^k$  results. This can be done in several different ways. In Ref. 16 it has been shown that a reasonable approximation to first-order corrections is to replace the  $\alpha_s(p_T^2)$  in the  $\hat{\sigma}_{ij}^k$ 's by  $\alpha_s(0.075 p_T^2)$ ; this is the recipe that will be adopted when needed.

A reasonable measure for the “hardness” of a parton-parton interaction is provided by the  $p_T^2$  scale. The differential cross section as a function of  $p_T^2$  is given by

$$\frac{d\sigma}{dp_T^2} = \sum_{i,j,k} \int \int \int dx_1 dx_2 d\hat{t} \hat{\sigma}^k(\hat{s}, \hat{t}, \hat{u}) f_i^1(x_1, Q^2) f_j^2(x_2, Q^2) \delta \left( p_T^2 - \frac{\hat{t} \hat{u}}{\hat{s}} \right) \quad (3)$$

and the hard-scattering cross section above some  $p_{T\min}$  by

$$\sigma_{\text{hard}}(p_{T\min}) = \int_{p_{T\min}^2}^{s/4} \frac{d\sigma}{dp_T^2} dp_T^2. \quad (4)$$

Since the differential cross section diverges roughly like  $dp_T^2/p_T^4$ ,  $\sigma_{\text{hard}}$  is also divergent for  $p_{T\min} \rightarrow 0$ . This is illustrated in Fig. 1 for a few different c.m. energies.

There are two potential major sources of error to the results in Fig. 1. First, the “dense packing” problem:<sup>17</sup> at small  $x$  values the effective number of partons in a hadron can grow so fast that not all fit inside the hadron. Then parton recombination effects become important, and the standard Altarelli-Parisi evolution of structure functions is no longer valid. Fortunately, it has been shown<sup>18</sup> that  $p_{T\min}$  values around or above 2 GeV are safe all the way up to Superconducting Super Collider (SSC) energies. Second, the shape of the structure functions at small  $x$

and small  $Q^2$  values is given neither by experiment nor by theory. Different reasonable *Ansätze* could well give an order of magnitude difference for the  $\sigma_{\text{hard}}(p_{T\min} = 2 \text{ GeV})$  at 40 TeV (Ref. 19). In our calculations, the effective shape at small  $x$  is roughly  $x^{-1}$ , but arguments have been raised for a behavior more like  $x^{-1.3}$  (Ref. 20).

At present collider energies,  $\sigma_{\text{hard}}(p_{T\min})$  becomes comparable with the total cross-section for  $p_{T\min} \approx 1.5 - 2$  GeV. This need not lead to contradictions:  $\sigma_{\text{hard}}$  does not give the hadron-hadron cross section but the parton-parton one. Each of the incoming hadrons may be viewed as a beam of partons, with the possibility of having several parton-parton interactions when the hadrons pass through each other. In this language,  $\sigma_{\text{hard}}(p_{T\min})/\sigma_{\text{tot}}$  is simply the average number per event of parton-parton scatterings above  $p_{T\min}$ , and this number may well be larger than unity.

While the introduction of several interactions per event

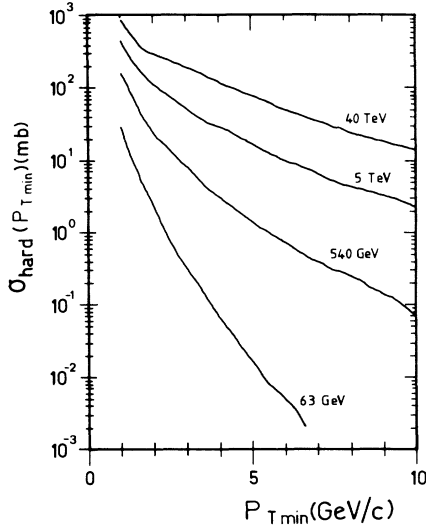


FIG. 1. The integrated parton-parton cross section  $\sigma_{\text{hard}}(p_{T\text{min}})$  as a function of the  $p_{T\text{min}}$  cutoff scale. Curves are, from bottom to top, for 63 GeV, 540 GeV, 5 TeV, and 40 TeV, respectively. No effective  $K$  factors are included here.

is the natural consequence of allowing small  $p_{T\text{min}}$  values and hence large  $\sigma_{\text{hard}}$  ones, it is not the solution of  $\sigma_{\text{hard}}(p_{T\text{min}})$  being divergent for  $p_{T\text{min}} \rightarrow 0$ : the average  $\hat{s}$  of a scattering decreases slower with  $p_{T\text{min}}$  than the number of interactions increases, so naively the total amount of scattered partonic energy becomes infinite. One cutoff is therefore obtained via the need to introduce proper multiparton correlated structure functions inside a hadron. This is not a part of the standard perturbative QCD formalism and is therefore not built into Eq. (4). In practice, it seems to be too weak a cut; i.e., it leads to a picture with too little of the incoming energy remaining in the small-angle beam jet region.

A more credible reason for an effective cutoff is that the incoming hadrons are color-neutral objects. Therefore, when the  $p_T$  of an exchanged gluon is made small and the transverse wavelength correspondingly large, the gluon can no longer resolve the individual color charges, and the effective coupling is decreased. This mechanism is not in contradiction to perturbative QCD calculations, which are always performed assuming scattering of free partons (rather than partons inside hadrons), but neither does present knowledge of QCD provide an understanding of how such a decoupling mechanism would work in detail. For the purpose of this section, a sharp cutoff at some energy-independent  $p_{T\text{min}}$  scale will be used, i.e., it will be assumed that  $d\sigma/dp_T^2 = 0$  for  $p_T < p_{T\text{min}}$ . The issue will be further discussed in Sec. IV.

Finally, a word about total cross sections. The  $\sigma_{\text{tot}}$  of hadron-hadron interactions is conveniently subdivided into a number of terms:

$$\sigma_{\text{tot}}(s) = \sigma_{\text{el}}(s) + \sigma_{\text{SD}}(s) + \sigma_{\text{DD}}(s) + \sigma_{\text{ND}}(s), \quad (5)$$

where  $\sigma_{\text{el}}$  is the elastic cross section,  $\sigma_{\text{SD}}$  the single-diffractive one,  $\sigma_{\text{DD}}$  the double-diffractive one, and  $\sigma_{\text{ND}}$  the nondiffractive, inelastic one. It is the latter class of “ordinary multihadronic events” that this paper sets out to study, and a knowledge of  $\sigma_{\text{ND}}(s)$  is therefore required. In this paper, we have used the Block-Cahn set-1 parametrization for  $\sigma_{\text{tot}}(s)$  and  $\sigma_{\text{el}}(s)$  (Ref. 21), and diffractive cross sections are given by the *Ansatz* of Goulianos.<sup>22</sup> This leaves a  $\sigma_{\text{ND}}$  of roughly 40 mb at 600 GeV and 100 mb at 40 TeV.

## B. The multiple-interaction formalism

In an event with several interactions, it is convenient to impose an ordering. The logical choice is to arrange the scatterings in falling sequence of  $x_T = 2p_T/s^{1/2}$ . The “first” scattering is thus the hardest one, with the “subsequent” (“second,” “third,” etc.) successively softer. It is important to remember that this terminology is in no way related to any picture in physical time; we do not know anything about the latter. In principle, all the scatterings that occur in an event must be correlated somehow, naively by momentum and flavor conservation for the partons from each incoming hadron, less naively by various quantum-mechanical effects. When averaging over all configurations of soft partons, however, one should effectively obtain the standard QCD phenomenology for a hard scattering, e.g., in terms of structure functions. Correlation effects, known or estimated, can be introduced in the choice of subsequent scatterings, given that the “preceding” (harder) ones are already known.

With a total cross section of hard interactions  $\sigma_{\text{hard}}(p_{T\text{min}})$  to be distributed among  $\sigma_{\text{ND}}(s)$  (nondiffractive, inelastic) events, the average number of interactions per event is just the ratio  $\sigma_{\text{hard}}(p_{T\text{min}})/\sigma_{\text{ND}}(s)$ . As a starting point we will assume that all hadron collisions are equivalent (no impact-parameter dependence), and that the different parton-parton interactions take place completely independently of each other. The number of scatterings per event is then distributed according to a Poissonian distribution with mean  $\sigma_{\text{hard}}(p_{T\text{min}})/\sigma_{\text{ND}}(s)$ . For Monte Carlo generation of these interactions it is useful to define

$$p(x_T) = \frac{1}{\sigma_{\text{ND}}(s)} \frac{d\sigma}{dx_T}, \quad (6)$$

with  $d\sigma/dx_T$  obtained by analogy with Eq. (3). Then  $p(x_T)$  is simply the probability to have a parton-parton interaction at  $x_T$ , given that the two hadrons undergo a nondiffractive, inelastic collision.

The probability that the hardest interaction, i.e., the one with highest  $x_T$ , is at  $x_{T1}$ , is now given by

$$p(x_{T1}) \exp \left[ - \int_{x_{T1}}^1 p(x'_T) dx'_T \right], \quad (7)$$

i.e., the naive probability to have a scattering at  $x_{T1}$  multiplied by the probability that there was no scattering with  $x_T$  larger than  $x_{T1}$ . Correspondingly, the probability to have the second hardest scattering at  $x_{T2}$  is given by

$$\int_{x_{T2}}^1 dx_{T1} \exp \left[ - \int_{x_{T1}}^1 p(x'_T) dx'_T \right] p(x_{T1}) \exp \left[ - \int_{x_{T2}}^{x_{T1}} p(x'_T) dx'_T \right] p(x_{T2}) \\ = p(x_{T2}) \left[ \int_{x_{T2}}^1 p(x'_T) dx'_T \right] \exp \left[ - \int_{x_{T2}}^1 p(x'_T) dx'_T \right], \quad (8)$$

i.e., the product of the probabilities to have no scattering between 1 and  $x_{T1}$ , to have one at  $x_{T1}$ , to have none between  $x_{T1}$  and  $x_{T2}$  and to have one at  $x_{T2}$ , integrated over all possible  $x_{T1}$ . In general, for the  $n$ th scattering, the exponentials always sum up to give the integral between  $x_{Tn}$  and 1. The nested integral over scatterings  $x_{T1} > x_{T2} > \dots > x_{T(n-1)} > x_{Tn}$  is given by

$$\int_{x_{Tn}}^1 dx_{T1} p(x_{T1}) \int_{x_{Tn}}^{x_{T1}} dx_{T2} p(x_{T2}) \dots \int_{x_{Tn}}^{x_{T(n-1)}} dx_{T(n-1)} p(x_{T(n-1)}) = \frac{1}{(n-1)!} \left[ \int_{x_{Tn}}^1 p(x'_T) dx'_T \right]^{n-1}, \quad (9)$$

so that the probability for an  $n$ th scattering at  $x_{Tn}$  becomes

$$p(x_{Tn}) \frac{1}{(n-1)!} \left[ \int_{x_{Tn}}^1 p(x'_T) dx'_T \right]^{n-1} \exp \left[ - \int_{x_{Tn}}^1 p(x'_T) dx'_T \right]. \quad (10)$$

The total probability to have a scattering at  $x_T$ , irrespectively of it being the first, second, or whatever, obviously is

$$\sum_{n=1}^{\infty} p(x_T) \frac{1}{(n-1)!} \left[ \int_{x_T}^1 dx'_T p(x'_T) \right]^{n-1} \exp \left[ - \int_{x_T}^1 dx'_T p(x'_T) \right] = p(x_T). \quad (11)$$

The multiple-interaction formalism thus retains the correct perturbative QCD expression for the scattering probability at any given  $x_T$ .

With the help of the integral

$$P(x_T) = \int_{x_T}^1 p(x'_T) dx'_T \\ = \frac{1}{\sigma_{\text{ND}}} \int_{sx_T^{2/4}}^{s/4} \frac{d\sigma}{dp_T^2} dp_T^2 \quad (12)$$

[where we assume  $P(x_T) \rightarrow \infty$  for  $x_T \rightarrow 0$ ] and its inverse  $P^{-1}$ , the iterative procedure to generate a chain of scatterings  $x_{T1} > x_{T2} > \dots$  is described by

$$x_{Ti} = P^{-1} [P(x_{T(i-1)}) - \ln R_i]. \quad (13)$$

Here the  $R_i$  are random numbers evenly distributed between 0 and 1. The iterative chain is started with a fictitious  $x_{T0} = 1$  and is terminated when  $x_{Ti}$  is smaller than  $x_{T\text{min}} = 2p_{T\text{min}}/s^{1/2}$ . Since  $P$  and  $P^{-1}$  are not known analytically, the standard Monte Carlo procedure is to find a  $\bar{p}(x_T) \geq p(x_T)$  for all  $x_T > x_{T\text{min}}$ , with  $\bar{p}$  a particularly simple function, such as  $\text{const}/x_T^3$  (i.e., using the approximate  $dp_T^2/p_T^4$  behavior noted earlier), which can be analytically integrated and inverted. From the chain generated with the use of  $\bar{p}(x_T)$ , a given  $x_{Ti}$  is to be retained with probability  $p(x_{Ti})/\bar{p}(x_{Ti})$ .

In addition, for each  $x_T$  value chosen, further variables have to be found according to the matrix element. This involves selecting  $\tau = x_1 x_2$  and  $x_F = x_1 - x_2$  for each incoming parton pair, resolving the twofold ambiguity between  $\hat{t}$  and  $x_T$ :

$$\hat{t} = -\frac{1}{2}\hat{s} \left[ 1 \pm \left[ 1 - \frac{x_T^2}{\tau} \right]^{1/2} \right], \quad (14)$$

choosing flavors for the incoming partons and, where necessary, for the outgoing ones. All this can be handled using standard Monte Carlo techniques, in particular by generalizing  $p(x_T)$  and  $\bar{p}(x_T)$  above to be functions also of  $\tau$ ,  $x_F$ , etc.

Whereas the ordinary structure functions should be used for the hardest scattering in order to reproduce standard QCD phenomenology, the structure functions to be used for subsequent scatterings must depend on all preceding  $x$  values and flavors chosen. We do not know enough about the hadron wave function to write down such joint probability distributions (some suggestions are round in Refs. 23, 24, 6, and 7). To take into account the energy ‘‘already’’ used in harder scatterings, a conservative approach is to evaluate the structure functions, not at  $x_n^a$  for the  $n$ th scattered parton from hadron  $a$  but at

$$x_n^{ia} = \frac{x_n^a}{1 - \sum_{i=1}^{n-1} x_i^a}. \quad (15)$$

This will be our standard procedure in the following; we have tried a few alternatives without finding any significantly different behavior in the final physics.

### C. Further model details

In a fraction  $\exp[-P(x_{T\text{min}})]$  of the events studied, there will be no hard scattering above  $x_{T\text{min}}$  when the iterative procedure in Eq. (13) is applied. It is therefore also necessary to have a model for what happens in events with no (semi)hard interactions. The simplest possible way to produce an event is to have an exchange of a very soft gluon between the two colliding hadrons. Without (initially) affecting the momentum distribution of partons, the ‘‘hadrons’’ become color-octet objects rather than color-singlet ones. If only valence quarks are considered, the color-octet state of a baryon can be decomposed into a color-triplet quark and an antitriplet diquark. In a baryon-baryon collision, one would then obtain a two-string picture,<sup>25</sup> with each string stretched from the quark of one baryon to the diquark of the other, Fig. 2(a). A baryon-antibaryon collision would give one string between a quark and an antiquark and another one between a diquark and an antiquark, Fig. 2(b).

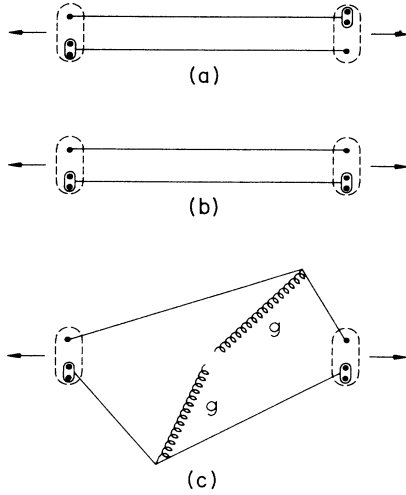


FIG. 2. Schematic view of color string drawing in hadron collisions. Solid lines indicate strings, dashed outline indicates outgoing hadron remnants, with a dot for each valence quark (antiquark) and an extra ellipse marking an effective diquark (antidiquark). (a) Baryon-baryon collision. (b) Baryon-antibaryon collision. (c) Baryon-antibaryon collision containing a hard gluon-gluon scattering.

It remains to be specified how the two strings should share the available energy. Following Ref. 24 one may, e.g., choose an *Ansatz*

$$P(\chi) = \frac{(1-\chi)^2}{(\chi^2 + c^2)^{1/4}} \quad (16)$$

for the fraction  $\chi$  that the quark takes of the baryon energy, with  $1-\chi$  taken by the diquark. The cutoff  $c = 2m_q/s^{1/2} \approx 0.6 \text{ GeV}/s^{1/2}$  is not really necessary here, but is included for further reference.

If an event contains a hard interaction, the string-drawing issues become more complicated, since there may be many ways of connecting the color charges of the outgoing objects. Furthermore, the standard QCD cross sections cannot be uniquely split into a sum of terms, where each term corresponds to a well-defined color flow, since also interference terms are present. These interference terms are suppressed by  $1/N_C^2$ , where  $N_C = 3$  is the number of colors. By neglecting the interference terms, it is possible to obtain a consistent scheme for selecting the string drawing in a given event.<sup>26</sup> One possible string drawing for  $gg \rightarrow gg$  scattering is shown in Fig. 2(c). This string drawing, as well as all other one-gluon-exchange processes between gluons and valence quarks, reduce to the simple low- $p_T$  two-string picture when the  $p_T$  of the hard scattering vanishes.

When several hard scatterings are present in an event, string-drawing issues become even more complicated. Specifically, the string drawing now depends on the relative color arrangement, in each hadron individually, of the partons that are about to scatter. This is a subject about which nothing is known. Many scenarios could therefore be envisioned. The simplest is to assume that, following the hardest interaction, all subsequent ones are of the  $gg \rightarrow gg$  type, with the two gluons in a color-

singlet state. Then each interaction will result in a double string being stretched directly between the two outgoing gluons, decoupled from the rest of the system. Only the hardest interaction gives strings coupled to the beam remnants. This is the solution adopted for the moment, with further alternatives to be discussed in Sec. IV D. While details are sensitive to the choice made, the overall picture is surprisingly stable, as will be shown later.

With the energy of scattered partons subtracted, Eq. (16) could still be used to give the sharing of remaining energy between the quark and diquark. If several interactions are to be allowed per event, this tends to lead to a too high average charged multiplicity, so in the multiple-interaction scenario Eq. (16) is replaced by the structure-function-inspired

$$P(\chi) = \frac{(1-\chi)^3}{(\chi^2 + c^2)^{1/2}} \quad (17)$$

throughout.

A hard interaction between colored objects is, by necessity, associated with the possibility of having initial- and final-state radiation. For technical reasons, this is included here only for the hardest interaction. In practice, there is no problem: except for the hardest interaction, which can be hard because of experimental trigger conditions, it is unlikely for a parton scattering to be so hard that radiation plays a significant role. The final-state radiation formalism used is the one presented in Ref. 27, including coherence effects,<sup>28</sup> while initial-state radiation is described with the help of the “backwards evolution” formalism developed in Ref. 29. In the context of the leading-logarithmic-type parton showers thus described, the string drawing is straightforward.

Given a set of outgoing colored partons, with information about how these partons are connected via strings, the Lund string-fragmentation model<sup>30</sup> provides a description of the subsequent hadronization. In its Monte Carlo implementation,<sup>4</sup> the developments of Ref. 31 are of vital importance, including as they do the treatment of very complicated partonic states, where some string pieces may also have rather small invariant masses.

### III. RESULTS WITH NO IMPACT-PARAMETER DEPENDENCE

In this section we wish to give a brief review of the shortcomings of some simple models for hadronic events, with and without multiple interactions. This will provide the incentive for introducing an impact-parameter picture in the next section.

#### A. The simple two-string picture

The simplest possible model for hadronic events is the two-string picture described in Sec. II C. There are no hard interactions at all, and the only degrees of freedom are the two  $\chi$  variables, which determine the masses of the two string systems.

In Fig. 3 this model is compared with the UA5 acceptance-corrected data on the charged-multiplicity distribution for 540-GeV  $p\bar{p}$  events.<sup>32</sup> It is immediately not-

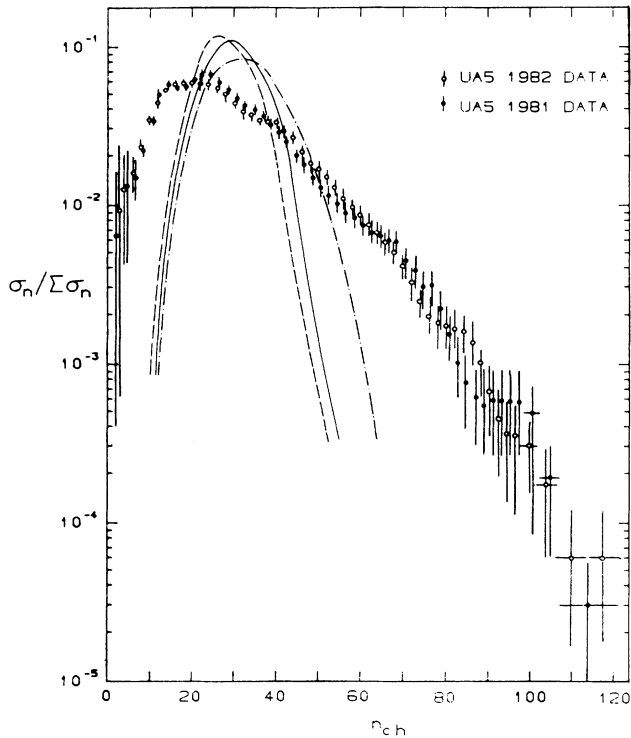


FIG. 3. Charged-multiplicity distribution at 540 GeV, UA5 results (Ref. 32) vs simple models: dashed low  $p_T$  only, full including hard scatterings, dash-dotted also including initial- and final-state radiation.

ed that the model gives far too narrow a distribution. This is basically the statement that multiplicity distributions in  $e^+e^-$  annihilation are much more narrow than in hadron physics. Comparing the two-string hadronic events with the  $e^+e^-$  one-string ones, the fluctuation of string masses in the former does broaden the distribution, but nowhere near enough.

Another interesting observable is the forward-backward correlation, defined in the following way. Consider two bins in pseudorapidity: one between  $\Delta\eta/2$  and  $\Delta\eta/2+1$  (forward), the other between  $-\Delta\eta/2$  and  $-(\Delta\eta/2+1)$  (backward), i.e., two one-unit-wide bins separated by a central gap of  $\Delta\eta$ . Call the charged multiplicities in the two bins  $n_F$  and  $n_B$ , and define the correlation coefficient by

$$b = \frac{\langle n_F n_B \rangle - \langle n_F \rangle^2}{\langle n_F^2 \rangle - \langle n_F \rangle^2} \quad (18)$$

(for  $\langle n_B \rangle = \langle n_F \rangle$  and  $\langle n_B^2 \rangle = \langle n_F^2 \rangle$ ). In Fig. 4 the correlation coefficient  $b$  is plotted as a function of  $\Delta\eta$ , again comparing the model with UA5 data.<sup>33</sup> Apart from a very small short-range effect, the model does not predict any forward-backward correlations.

### B. Introduction of hard interactions

A model that only contains partons with small transverse momenta is obviously a simplification. With a sharp cutoff of the perturbative two-jet cross section at

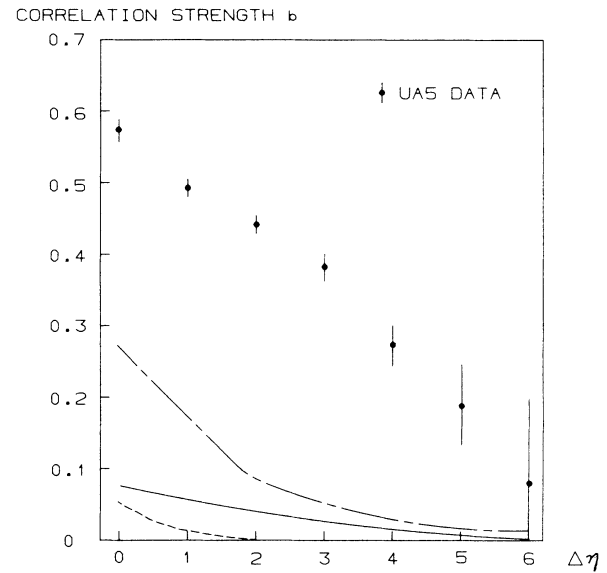


FIG. 4. Forward-backward multiplicity correlation at 540 GeV, UA5 results (Ref. 33) vs simple models; the latter models with notation as in Fig. 3.

$p_{T\min} = 1.8$  GeV, roughly two-thirds of all events would be expected to contain a hard interaction. The remaining  $\frac{1}{3}$  is still assumed to be low  $p_T$ .

The inclusion of hard interactions actually results in negligible improvements of Figs. 3 and 4. The reason is that most “hard” interactions still have a  $p_T$  for the scattered partons in the range 2–3 GeV, i.e., not enough to make a difference in the event structure.

If initial- and final-state radiation effects are included, some further improvements are noted in Figs. 3 and 4. Again the soft nature of most interactions makes the effect less than adequate, however.

Whereas some uncertainty may be present in the details of what is included up to this point, even rather drastic variations are insufficient to come anywhere near an explanation of the data.

### C. Effects of multiple interactions

Multiple interactions are now introduced above some given  $p_{T\min}$  scale, using the formalism explained in Sec. II B. Events which do not give any interactions above  $p_{T\min}$  are again classified as two-string low- $p_T$  events.

There is thus one main free parameter in the problem:  $p_{T\min}$ . As  $p_{T\min}$  is decreased, the average number of interactions is increased, and so are the fluctuations in this number. Events which contain a large number of interactions also have large multiplicities. In Fig. 5 it is shown how the multiplicity distribution evolves as  $p_{T\min}$  is decreased from 2.0 to 1.6 to 1.2 GeV. At the same time, the average number of interactions per event is increased from 0.56 to 1.01 to 2.11. A fair agreement with the high-multiplicity tail is obtained for  $p_{T\min} = 1.6$  GeV. With an energy sharing between diquark and quark given by Eq. (17), the  $\langle n_{ch} \rangle$  values go from 29 to 33 to

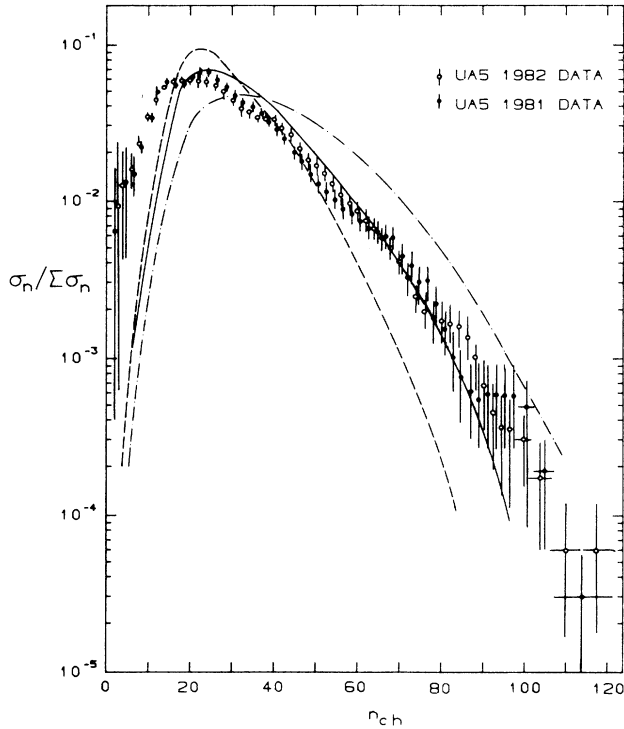


FIG. 5. Charged-multiplicity distribution at 540 GeV, UA5 results (Ref. 32) vs impact-parameter-independent multiple-interaction model: dashed line,  $p_{Tmin}=2.0$  GeV; solid line,  $p_{Tmin}=1.6$  GeV; dashed-dotted line,  $p_{Tmin}=1.2$  GeV.

42. Compared with the UA5 figure of  $\langle n_{ch} \rangle \approx 29$  (Ref. 32), only the first two  $p_{Tmin}$  values are acceptable. If instead the energy sharing is given by Eq. (16), corresponding to a higher  $\langle n_{ch} \rangle$  before any hard interactions at all are introduced, only the highest  $p_{Tmin}$  value would give an acceptable  $\langle n_{ch} \rangle$ , but then without reproducing the high-multiplicity tail.

With multiple interactions included, the forward-backward correlations are of significant size, Fig. 6, since the number of scatterings strongly influences the multiplicity in both hemispheres simultaneously. Also several other observations, e.g., the rate of “hot spots”,<sup>34</sup> are now understood.

There are other places where this scenario fails, however. One is that it underestimates the energy away from the core of a jet, Fig. 7, i.e., there is not a large enough “pedestal effect” in the model. This would seem to imply that events containing one hard interaction also contain an above-average amount of extra semihard interactions, i.e., effects of varying impact parameters.

#### IV. THE MODEL WITH VARIABLE IMPACT PARAMETERS

Up to this point, it has been assumed that the initial state is the same for all hadron collisions, whereas in fact each collision also is characterized by a varying impact parameter  $b$ . Within the classical framework of this paper,  $b$  is to be thought of as a distance of closest approach,

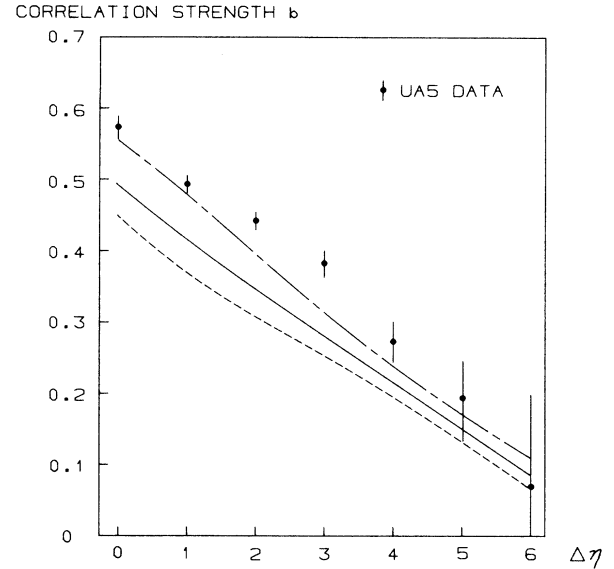


FIG. 6. Forward-backward multiplicity correlation at 540 GeV, UA5 results (Ref. 33) vs impact-parameter-independent multiple-interaction model; the latter with notation as in Fig. 5.

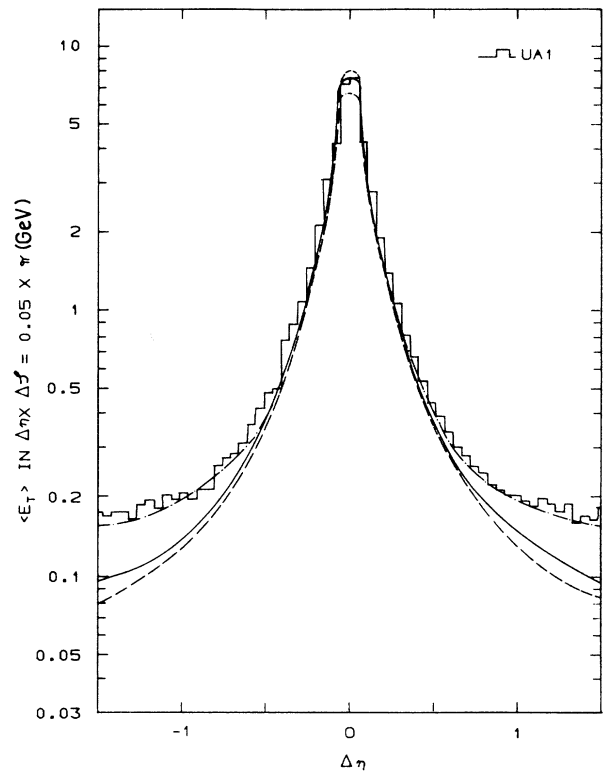


FIG. 7. Jet energy profile for  $E_{Tjet} > 35$  GeV at 540 GeV, UA1 data (Ref. 35) vs model results: dashed line, without multiple interactions; solid line, with multiple interactions (impact-parameter independent); dashed-dotted line, with multiple-interaction rate arbitrarily increased by a factor of 4.

not as the Fourier transform of the momentum transfer. A small  $b$  value corresponds to a large overlap between the two colliding hadrons, and hence an enhanced probability for multiple interactions. A large  $b$ , on the other hand, corresponds to a grazing collision, with a large probability that no parton-parton interactions at all take place.

### A. The hadronic matter distribution

In order to quantify the concept of hadronic matter overlap, one may assume a spherically symmetric distribution of matter inside the hadron,  $\rho(\bar{x})d^3x = \rho(r)d^3x$ . For simplicity, the same spatial distribution is taken to apply for all parton species and momenta. Four different parametrizations of the matter distribution have been compared, to check how sensitive results are to this choice. The first three are a solid sphere  $\rho_1(r) \propto \theta(a-r)$ , a Gaussian  $\rho_2(r) \propto \exp(-r^2/a^2)$  and an exponential  $\rho_3(r) \propto \exp(-r/a)$ . Since differences in physics results between these three turned out to be smaller than anticipated, and since none of them gave a sufficiently large pedestal effect, the fourth possibility was chosen to be a double Gaussian:

$$\rho_4(r) \propto (1-\beta) \frac{1}{a_1^3} \exp\left[-\frac{r^2}{a_1^2}\right] + \beta \frac{1}{a_2^3} \exp\left[-\frac{r^2}{a_2^2}\right]. \quad (19)$$

This corresponds to a distribution with a small core region, of radius  $a_2$  and containing a fraction  $\beta$  of the total hadronic matter, embedded in a larger hadron of radius  $a_1$ . While it is mathematically convenient to have the origin of the two Gaussians coinciding, the physics could well correspond to having three disjoint core regions, reflecting the presence of three valence quarks, together carrying the fraction  $\beta$ . One could alternatively imagine a hard hadronic core surrounded by a pion cloud, as in the chiral bag model.<sup>36</sup> To be specific, the values  $\beta=0.5$  and  $a_1/a_2=5$  have been used throughout this paper. The double Gaussian will be used as the standard matter distribution in the following. It should be noted that the overall distance scale  $a$  (or  $a_1$ ) never enters in the subsequent calculations, since the inelastic, nondiffractive cross section  $\sigma_{\text{ND}}(s)$  is taken from literature rather than calculated from the  $\rho(r)$ .

For a collision with impact parameter  $b$ , the time-integrated overlap between the matter distributions of the colliding hadrons is given by

$$\bar{O}(b) = \int \int d^3x dt \rho_{\text{boosted}}\left[x - \frac{b}{2}, y, z - vt\right] \rho_{\text{boosted}}\left[x + \frac{b}{2}, y, z + vt\right], \quad (20)$$

where  $v$  is the velocity in the c.m. frame and  $\rho_{\text{boosted}}$  the suitably Lorentz contracted  $\rho(\bar{x})$ . By a scale change in  $z$ ,  $\rho_{\text{boosted}}$  can be replaced by  $\rho$ . After a further scale change in  $t$  one obtains

$$\bar{O}(b) \propto \int \int d^3x dt \rho\left[x - \frac{b}{2}, y, z - \frac{t}{2}\right] \rho\left[x + \frac{b}{2}, y, z + \frac{t}{2}\right] = \int dt \int d^3x \rho(x, y, z) \rho(x, y, z - (b^2 + t^2)^{1/2}). \quad (21)$$

As an example, the double Gaussian of Eq. (19) gives

$$\begin{aligned} \bar{O}_4(b) \propto & (1-\beta)^2 \frac{1}{2a_1^2} \exp\left[-\frac{b^2}{2a_1^2}\right] \\ & + 2\beta(1-\beta) \frac{1}{a_1^2 + a_2^2} \exp\left[-\frac{b^2}{a_1^2 + a_2^2}\right] \\ & + \beta^2 \frac{1}{2a_2^2} \exp\left[-\frac{b^2}{2a_2^2}\right]. \end{aligned} \quad (22)$$

In addition to the  $\bar{O}(b)$  obtained with the  $\rho_1$ – $\rho_4$  above, it is useful to have an alternative  $\bar{O}_0(b) \propto \theta(a-b)$ , i.e., where all events have the same overlap. This may be thought of as collisions at an average, fixed impact parameter. It will not be exactly equivalent to the formalism of Sec. II, for reasons that will become apparent.

The overlap  $\bar{O}(b)$  is obviously strongly related to the eikonal  $\Omega(b)$  of optical models. We have kept a separate notation, since the physics context of the two is slightly different:  $\Omega(b)$  is based on the quantum-mechanical scattering of waves in a potential, and is normally used to describe the elastic scattering of a hadron as a whole, while  $\bar{O}(b)$  comes from a purely classical picture of point-

like partons distributed inside the two colliding hadrons. Furthermore, the normalization and energy dependence is differently realized in the two formalisms.

### B. The variable-impact-parameter formalism

The larger the overlap  $\bar{O}(b)$  is, the more likely it is to have interactions between partons in the two colliding hadrons. In fact, there should be a linear relationship

$$\langle \bar{n}(b) \rangle = k \bar{O}(b), \quad (23)$$

where  $\bar{n}=0, 1, 2, 3, \dots$  counts the number of interactions when two hadrons pass each other with an impact parameter  $b$ . The constant of proportionality  $k$ , is related to the parton-parton cross section and hence increases with c.m. energy.

For each given impact parameter, the number of interactions is assumed to be distributed according to a Poissonian distribution. If the matter distribution has a tail to infinity (which is true for the examples above, except for the solid sphere), events may be obtained with arbitrarily large  $b$  values. In order to obtain finite total cross sections, it is necessary to assume that each event

contains at least one semihard interaction. The probability that two hadrons, passing each other with an impact parameter  $b$ , will actually undergo a collision is then given by

$$P_{\text{int}}(b) = 1 - e^{-\langle \bar{n}(b) \rangle} = 1 - e^{-k\bar{O}(b)} \quad (24)$$

according to Poissonian statistics. The average number of interactions per event at impact parameter  $b$  is now

$$\langle n(b) \rangle = \frac{\langle \bar{n}(b) \rangle}{P_{\text{int}}(b)} = \frac{k\bar{O}(b)}{1 - \exp[-k\bar{O}(b)]}, \quad (25)$$

where the denominator comes from the removal of hadrons which passed without colliding, i.e., with  $\bar{n} = 0$ .

In Sec. II, the relationship  $\langle n \rangle = \sigma_{\text{hard}}/\sigma_{\text{ND}}$  was introduced for the average number of interactions per nondiffractive, inelastic event. When averaged over all impact parameters, this relation must still hold true: the introduction of variable impact parameters may give more interactions in some events and less in others, but it does not affect either  $\sigma_{\text{hard}}$  or  $\sigma_{\text{ND}}$ . For the former this is because the perturbative QCD calculations only depend on the total parton flux, for the latter by construction. Integrating Eq. (25) over  $b$  one then obtains

$$\begin{aligned} \langle n \rangle &= \frac{\int \langle n(b) \rangle P_{\text{int}}(b) d^2b}{\int P_{\text{int}}(b) d^2b} \\ &= \frac{\int k\bar{O}(b) d^2b}{\int \{1 - \exp[-k\bar{O}(b)]\} d^2b} = \frac{\sigma_{\text{hard}}}{\sigma_{\text{ND}}}. \end{aligned} \quad (26)$$

For  $\bar{O}(b)$ ,  $\sigma_{\text{hard}}$ , and  $\sigma_{\text{ND}}$  given, with  $\sigma_{\text{hard}}/\sigma_{\text{ND}} > 1$ ,  $k$  can thus always be found (numerically) by solving the last equality.

The absolute normalization of  $\bar{O}(b)$  is not interesting in itself, but only the relative variation with impact parameter. It is therefore useful to introduce an ‘‘enhancement factor’’  $f(b)$ , which gauges how the interaction probability for a passage with impact parameter  $b$  compares with the average, i.e.,

$$\langle \bar{n}(b) \rangle = k\bar{O}(b) = f(b) \langle k\bar{O} \rangle. \quad (27)$$

In other words,

$$f(b) = \frac{\bar{O}(b)}{\langle \bar{O} \rangle} = \frac{\langle \bar{n}(b) \rangle}{\langle \bar{n} \rangle}. \quad (28)$$

The definition of the mean  $\langle \bar{O} \rangle$  is not unambiguous. With the choice to let  $\langle \bar{O} \rangle$  be the average of all events, i.e., where  $\bar{n} \geq 1$ ,

$$\langle \bar{O} \rangle = \frac{\int \bar{O}(b) P_{\text{int}}(b) d^2b}{\int P_{\text{int}}(b) d^2b}, \quad (29)$$

one obtains

$$\langle f \rangle = \frac{\int f(b) P_{\text{int}}(b) d^2b}{\int P_{\text{int}}(b) d^2b} = \frac{\int \bar{O}(b) P_{\text{int}}(b) d^2b}{\langle \bar{O} \rangle \int P_{\text{int}}(b) d^2b} = 1; \quad (30)$$

i.e., the average value of  $f(b)$  over all events is unity. A

large  $f$  value corresponds to a high probability for several interactions, while a small  $f$  corresponds to a peripheral collision with the minimal number of one interaction. The larger a tail the hadronic matter distribution has, or the more peaked it is at the origin, the wider the probability distribution in  $f$  is.

A further number needed in the following is

$$f_c = \frac{\int \bar{O}(b) P_{\text{int}}(b) d^2b}{\int \bar{O}(b) d^2b}, \quad (31)$$

which is impact-parameter independent. Typically  $f_c$  is somewhat smaller than 1, approaching unity from below when  $\sigma_{\text{hard}}/\sigma_{\text{ND}} \rightarrow \infty$ . The function of  $f_c$  will be to compensate for the fact that the average number of interactions per event is pushed up by the requirement that each event contain at least one interaction.

If Eqs. (27), (29), (31), and (26) are combined, one obtains

$$\begin{aligned} \langle \bar{n}(b) \rangle &= f(b) \langle k\bar{O} \rangle = f(b) \frac{\int k\bar{O}(b) P_{\text{int}}(b) d^2b}{\int P_{\text{int}}(b) d^2b} \\ &= f_c f(b) \frac{\int k\bar{O}(b) d^2b}{\int P_{\text{int}}(b) d^2b} \\ &= f_c f(b) \frac{\sigma_{\text{hard}}}{\sigma_{\text{ND}}}. \end{aligned} \quad (32)$$

This derivation, which has been given here for the total number of interactions for two hadrons passing each other at an impact parameter  $b$ , could equally well have been carried out for the number of interactions in a given  $p_T$  bin [since, contrary to the case  $n(b)$ , there is no constraint of the type  $\bar{n}(b) \geq 1$ ]. The conclusion is therefore that the effective probability  $p(x_T)$  of Eq. (6), giving the probability of having a scattering at  $x_T$ , should be replaced by

$$p(x_T, b) = f_c f(b) p(x_T) = f_c f(b) \frac{1}{\sigma_{\text{ND}}} \frac{d\sigma}{dx_T}. \quad (33)$$

The naive generation procedure is thus to pick a  $b$  according to the phase space  $d^2b$ , find the relevant  $f(b)$  and plug in the resulting  $p(x_T, b)$  in the formalism of Sec. II B. If at least one hard interaction is generated, the event is retained, or else a new  $b$  is to be found. This algorithm would work fine for hadronic matter distributions which vanish outside some radius, so that the  $d^2b$  phase space which needs to be probed is finite. Since this is not true for the distributions under study, it is necessary to do better.

### C. The event-generation formalism

By analogy with Eq. (7), it is possible to ask what the probability is to find the hardest scattering of an event at  $x_{T1}$ . For each impact parameter separately, the probability to have an interaction at  $x_{T1}$  is given by  $p(x_{T1}, b)$  in Eq. (33), and this should be multiplied by the probability that the event contains no interactions at a scale  $x'_T > x_{T1}$ ,

to yield the total probability distribution

$$\frac{dP_{\text{hardest}}}{d^2b dx_{T1}} = p(x_{T1}, b) \exp \left[ - \int_{x_{T1}}^1 p(x'_T, b) dx'_T \right]. \quad (34)$$

$$\begin{aligned} \frac{dP_{\geq 1}}{d^2b} &= \int_{x_{T\min}}^1 dx_T p(x_T, b) \exp \left[ - \int_{x_T}^1 p(x'_T, b) dx'_T \right] \\ &= 1 - \exp \left[ - \int_{x_{T\min}}^1 p(x'_T, b) dx'_T \right] = 1 - \exp \left[ -f_c f(b) \frac{\sigma_{\text{hard}}}{\sigma_{\text{ND}}} \right] = 1 - \exp[-k\bar{O}(b)] = P_{\text{int}}(b), \end{aligned} \quad (35)$$

in agreement with Eq. (24). A proper procedure would therefore be to select a  $b$  according to  $P_{\text{int}}(b)d^2b$ . This yields the  $f(b)$  value and hence the relevant  $p(x_T, b)$ . The  $p(x_T, b)$  can be directly plugged into the formalism of Sec. II B, to yield a sequence of  $x_{Ti}$  values for interactions. If no  $x_T$  values at all are found above  $x_{T\min}$ , which happens with probability  $\exp[-k\bar{O}(b)]$ , the interaction generation chain is to be restarted at  $x_{T0}=1$ , until a valid event (with  $\geq 1$  interaction) is found.

The procedure above is straightforward to implement, but it suffers from the disadvantage that it is only relevant for the generation of the inclusive sample of nondiffractive, inelastic events. In particular, it cannot be used to generate the activity accompanying a high- $p_T$  jet or a  $W$ , say, since such events are not distributed according to  $P_{\text{int}}(b)$ , but rather are biased towards smaller  $b$  values. The following trick can then be used.

If the treatment of the exponential in Eq. (34) is deferred for a moment, the equation reads

$$\frac{dP_{\text{hardest}}}{d^2b dx_{T1}} = p(x_{T1}, b) = f_c f(b) \frac{1}{\sigma_{\text{ND}}} \frac{d\sigma}{dx_T}(x_{T1}). \quad (36)$$

Here the distribution in  $b$  and  $x_{T1}$  appears in factorized form, so that the two can be chosen independently of each other. In particular, a high- $p_T$  jet or  $W$  can be chosen with whatever kinematics desired. For a  $W$  (or any  $s$ -channel resonance) there would be no obvious  $x_T$  scale by itself but, since  $x_T$  is used as a measure of the hardness of an interaction, a choice  $x_T^{-2} \approx \tau = \hat{s}/s$  is not unreasonable. With the  $b$  chosen according to  $f(b)d^2b$ , the neglected exponential

$$\begin{aligned} \exp \left[ - \int_{x_{T1}}^1 p(x'_T, b) dx'_T \right] \\ = \exp \left[ -f_c f(b) \int_{x_{T1}}^1 p(x'_T) dx'_T \right] \end{aligned} \quad (37)$$

can now be evaluated, and the event retained with a probability proportional to it. From the  $x_T$  scale of the selected interaction, a sequence of softer  $x_{Ti}$  values may again be generated as in Sec. II B, using the known  $p(x_T, b)$ . This sequence may be empty, i.e., the event need not contain any further interactions.

It is interesting to understand how the algorithm above works. By selecting  $b$  according to  $f(b)d^2b$ , i.e.,  $\bar{O}(b)d^2b$ , the primary  $b$  distribution is maximally biased towards small impact parameters. If the first interaction is hard, by choice of by chance, the integral of the cross

section above  $x_{T1}$  is small, and the exponential in Eq. (37) close to unity. Almost all events are therefore retained. The large  $f(b)$  value is also likely to lead to the generation of many further, softer interactions. If, on the other hand, the first interaction is not hard, the exponential is no longer close to unity, and many events are rejected. Since the exponent in Eq. (37) is proportional to  $f(b)$ , a large  $f(b)$  leads to an enhanced probability for rejection, whereas the chance of acceptance is larger with a small  $f(b)$ . Among events where the hardest interaction is soft, the  $b$  distribution is therefore biased towards larger values [smaller  $f(b)$ ], and there is a small probability for yet softer interactions.

#### D. Cross-section considerations

In this section, nothing has yet been assumed about the form of the  $d\sigma/dp_T$  spectrum. As in the impact-parameter-independent case, it is possible to use a sharp cutoff at some given  $p_{T\min}$  value. However, here each event is required to have at least one interaction, whereas before events without interactions were retained and set at  $p_T=0$ . It is therefore aesthetically more appealing to assume a more gradual turnoff, so that a (semi)hard interaction can be rather soft part of the time. The matrix elements roughly diverge like  $\alpha_s^2(p_T^2)dp_T^2/p_T^4$  for  $p_T \rightarrow 0$ . They could therefore be regularized as follows. First, to remove the  $1/p_T^4$  behavior, multiply by a factor  $p_T^4/(p_{T0}^2 + p_T^2)^2$ . Second, replace the  $p_T^2$  argument in  $\alpha_s$  by  $p_{T0}^2 + p_T^2$  or, with the inclusion of the  $K$  factor introduced in Sec. II A, replace  $0.075p_T^2$  by  $0.075(p_{T0}^2 + p_T^2)$ .

With these substitutions, a continuous  $p_T$  spectrum is obtained, stretching from  $p_T=0$  to  $s^{1/2}/2$ . For  $p_T \gg p_{T0}$  the standard perturbative QCD cross section is recovered, while values  $p_T \ll p_{T0}$  are strongly damped. The  $p_{T0}$  scale, which now is the main free parameter of the model, in practice comes out to be of the same order of magnitude as  $p_{T\min}$  did, i.e., roughly 2 GeV.

If gluons with large transverse wavelength decouple because of the color-singlet nature of hadrons, and if the transverse structure of hadrons is assumed to be energy independent, it is natural to assume that also  $p_{T\min}$  and  $p_{T0}$  are independent of the c.m. energy of the hadron collision. For the impact-parameter-independent picture this works out fine, with all events being reduced to low- $p_T$  two-string ones when the c.m. energy is reduced. In the variable-impact-parameter picture, the whole formalism

only makes sense if  $\sigma_{\text{hard}} > \sigma_{\text{ND}}$ , see, e.g., Eq. (26). Since  $\sigma_{\text{ND}}$  does not vanish with decreasing energy, but  $\sigma_{\text{hard}}$  would do that for a fixed  $p_{T0}$ , this means that  $p_{T0}$  has to be reduced when the energy is decreased.

It is reasonable to ask how meaningful the whole physics scenario becomes at small c.m. energies. The picture of multiple parton-parton interactions is certainly easier to visualize as a high-energy behavior, and as involving parton scatterings typically with a few GeV of transverse momentum. In the description of events at lower energies, where more emphasis would have to be put on interactions at small  $p_T$  values, the picture loses some of its luster. Possibly a physics description in other terms would be more sensible here: although the correct answer is unique, different approximations may do more or less well in a given region. Keeping this warning in mind, it is still meaningful to see what happens as the energy is varied.

Going a bit ahead of the story, the  $p_{T0}$  values at a given c.m. energy can be determined “simply” by the requirement that the mean charged multiplicity in the model should agree with the experimental one. Typical values obtained that way (with an uncertainty not only due to experimental errors, but also in the understanding of the relevant trigger conditions to use for Monte Carlo comparisons) are shown in Fig. 8 as a function of c.m. energy for the double Gaussian matter distribution. The increase of  $p_{T0}$  with energy is fairly slow, particularly for the higher energies. In the CERN  $S\bar{p}pS$  energy range, a logarithmic fit would give

$$p_{T0} = (2.0 \text{ GeV}) + (0.08 \text{ GeV}) \ln \left[ \frac{s^{1/2}}{540 \text{ GeV}} \right]. \quad (38)$$

If anything, an extrapolation of this trend would probably overestimate the  $p_{T0}$  at higher values. Taking the value at 540 GeV as a lower limit, this would suggest  $2.0 < p_{T0} < 2.35$  at 40 TeV. Although the variation of  $p_{T0}$  with energy in Eq. (38) is slow, the effect on the average number of interactions per event is rather drastic, leading to a considerably slower increase than is obtained with a fix  $p_{T0}$ , Fig. 9.

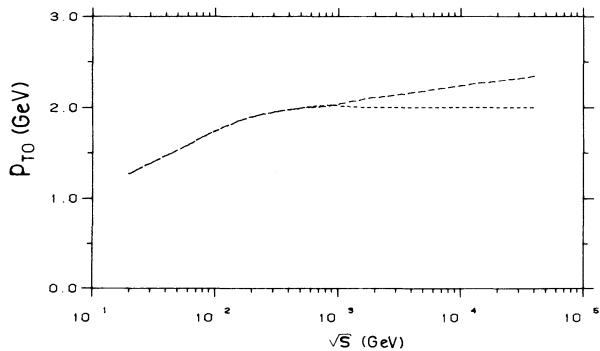


FIG. 8. Values for the cutoff parameter  $p_{T0}$  as a function of c.m. energy, as determined from comparisons with the average charged multiplicity. Dashed line, with a logarithmic extrapolation to higher energies, Eq. (38); dotted line, if assumed constant above 900 GeV.

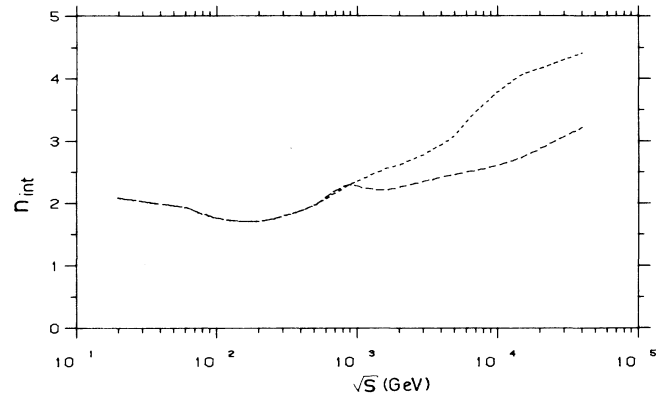


FIG. 9. The average number of interactions per nondiffractive event as a function of c.m. energy. Extrapolations shown correspond to the two extremes of Fig. 8.

While predicting cross sections is in no way the objective of this paper, it could still be interesting to see what the  $p_{T0}$  values determined above correspond to in terms of the inelastic, nondiffractive cross section  $\sigma_{\text{ND}}$ . Since no explicit scales have been introduced for the hadronic matter distribution, the absolute normalization is not known, but the energy dependence can be studied. In Fig. 10 the integral  $\int P_{\text{int}}(b) d^2b$  is shown, normalized to the parametrized  $\sigma_{\text{ND}}$  at 540 GeV. By and large, agreement with the parametrization is not that bad at higher energies, which at least shows that the model has some sense of internal consistency. The results at small energies are fairly unreliable: the multiplicity distribution is here more sensitive to variations in the string-drawing algorithm (specifically, to the method used for the hardest interaction) than to changes of  $p_{T0}$ . Furthermore, no sys-

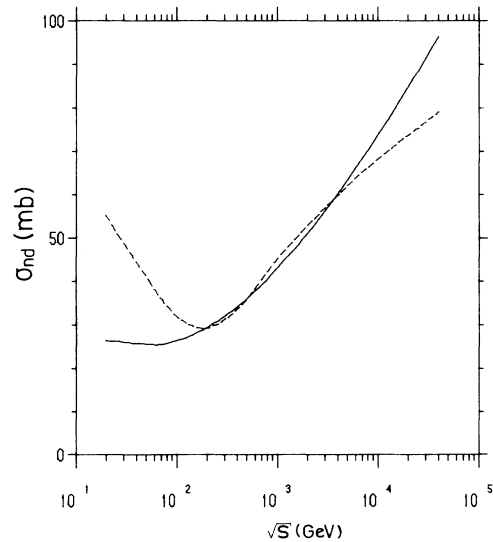


FIG. 10. Variation of the total inelastic, nondiffractive cross section obtained in the variable-impact-parameter picture, normalized to a standard parametrization (Refs. 21 and 22) at 540 GeV. Dashed line, model results (with  $p_{T0} = 2$  GeV above 900 GeV); full line, the parametrization.

tematic attempt has been made to study and correctly include the small differences in behavior between  $pp$  and  $p\bar{p}$  events.

### E. String-drawing issues

In Sec. II C, a description was given of one possible way of assigning flavors to and drawing strings between the scattered partons. In general, this formalism is retained. A few modifications have been introduced, however, as described in the following. It is not obvious *a priori* whether these are improvements or not, but this reflects the major uncertainties in this game.

With the introduction of a soft regularization of the cross section at  $p_T=0$ , many events come to contain the hardest interaction with a  $p_T$  in the region 0–1 GeV, i.e., fairly soft. Standard structure function parametrizations typically extend down to some  $Q_0$  scale in the order of 2 GeV. The normal procedure, to use the structure function values at  $Q_0$  whenever  $p_T \leq Q_0$ , may give an erroneous picture of the hadron at small  $Q^2$  scales. Specifically, it leads to a dominance of gluon-gluon scatterings over gluon-quark or quark-quark ones, whereas a not unreasonable scenario would have the valence quarks dominate the low- $Q^2$  hadron. We have therefore tried a simple recipe for enhancing the valence-quark content of the hadron at small  $p_T$ , as follows. With kinematics for the interaction chosen, a fraction  $p_{T0}^2/(p_{T0}^2+p_T^2)$  of the events is reassigned to correspond to a scattering between two valence quarks of the two incoming hadrons, while for the remaining fraction  $p_T^2/(p_{T0}^2+p_T^2)$ , flavors are chosen as usual. The kinematics of the hard interaction therefore replaces the selection of two  $\chi$  variables for most interactions at small  $p_T$  values.

In Sec. II C, it was assumed that all interactions after the hardest one were gluon-gluon scatterings, with the two gluons in a color-singlet state. Here a more realistic mix is introduced. One-third of all nonhardest interactions are assumed to be of the two-gluon type above, and an additional one-third are taken to give a string stretched between a  $q\bar{q}$  pair ( $q=u, d$  or  $s$ ). The final one-third are again gluon-gluon scatterings, but here color correlations are assumed such that each of the gluons should be connected onto one of the strings “already” present. Among the different possibilities of connecting the colors of the gluon, the one which minimizes the total increase in string length will be chosen. This is in contrast with the gluon-gluon closed-loop alternative, which roughly corresponds to a maximization of the extra string length. The three alternatives are illustrated in Fig. 11.

Sadly absent in the list above is the possibility that several of the valence quarks of the incoming hadrons interact independently of each other. While the scattering of one valence quark out of the baryon leaves a color-antitriplet diquark beam remnant carrying the baryon number, the scattering of a second valence quark is likely to set the baryon number in transverse motion. One simple scenario for this is to assume that the baryon is a Y-shaped string configuration, with a quark at each end point and the baryon number effectively associated with the junction point. If the ends are set in motion or

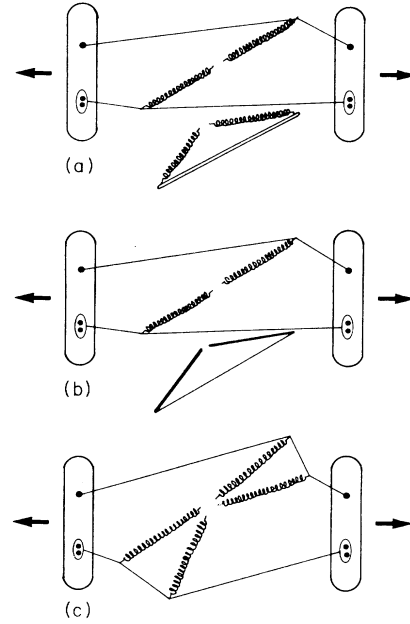


FIG. 11. Schematic view of the three string-drawing possibilities that are used, evenly mixed, to describe subsequent interactions. For notation cf. Fig. 2; in addition, thick solid lines denote scattered quarks. (a) Double string between scattered gluons. (b) Simple string between a scattered  $q\bar{q}$  pair. (c) Scattered gluons attached to nearby string pieces.

reattached by gluon exchanges, the junction point will start moving in a well-defined fashion<sup>37</sup> so as to minimize the total string length. As the three legs of the Y-shaped string start fragmenting, the baryon is going to be the one created around the junction. Without invoking any kind of “hard diquark scattering” mechanism,<sup>38</sup> this could well explain the abnormal rate of baryons at medium high  $p_T$  observed experimentally.<sup>39</sup> Unfortunately there is a catch: the fragmentation of a Y-shaped string is extremely difficult to handle in a consistent manner, and the problem has never been solved. We hope to return to this issue, and to a more realistic flavor composition of the nonhardest interactions, at a later date.

For the main features of events, like the one studied in this paper, the effects of the uncertainties involved should probably not be overemphasized. Whereas the three components above are usually evenly mixed, it is possible to study what happens if only one is used. Since the three represent different extremes, with the truth probably somewhere in between, it is comforting to note that a fair description of the data (but with different  $p_{T0}$  cutoffs) can be obtained with either of the three extreme possibilities.

In the multiplicity distributions shown in Sec. III, one of the problems always was that the model did not produce enough low-multiplicity events. Whereas the UA5 trigger conditions remove almost all single-diffractive events, most double-diffractive ones survive and are included in the multiplicity distributions. In the following, the generation of a diffractive events has therefore been included where relevant. This is made according to a simple model, with a  $dM^2/M^2$  spectrum for the mass of each

diffractive system. Each system is represented by a string stretched between a diquark in the forward end and a quark in the other one. Except for some tries with a double string stretched from a diquark and a quark in the forward direction to a central gluon, which gave only modest changes in the results, no attempts have been made with more detailed models for diffractive states.<sup>40</sup>

## V. MULTIPLICITY DISTRIBUTIONS

The charged-multiplicity distribution is interesting, despite its deceptive simplicity, since most physical mechanisms (of those playing a role in minimum bias events) contribute to the multiplicity buildup. This was illustrated in Sec. III. From now on we will use the complete model, i.e., including multiple interactions and varying impact parameters, to look more closely at the data. Single- and double-diffractive events are now also included; with the UA5 triggering conditions roughly  $\frac{3}{4}$  of the generated double-diffractive events are retained, while the contribution from single diffraction is negligible.

### A. Total multiplicities

A final comparison with the UA5 data at 540 GeV is presented in Fig. 12, for the double Gaussian matter distribution. The agreement is now generally good, although the value at the peak is still a bit high. In this distribution, the varying impact parameters do not play a major role; for comparison, Fig. 12 also includes the other ex-

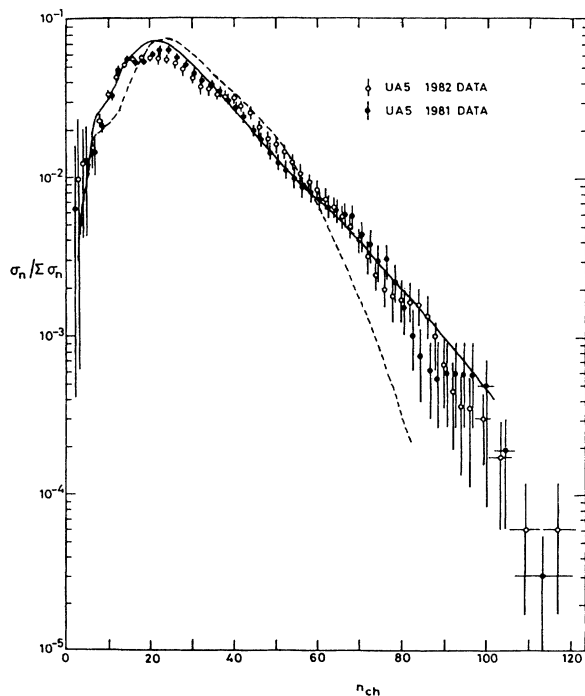


FIG. 12. Charged-multiplicity distribution at 540 GeV, UA5 results (Ref. 32) vs multiple-interaction model with variable impact parameter: solid line, double-Gaussian matter distribution; dashed line, with fix impact parameter [i.e.,  $\tilde{O}_0(b)$ ].

treme of a fix overlap  $\tilde{O}_0(b)$  (with the use of the formalism in Sec. IV, i.e., requiring at least one semihard interaction per event, so as to minimize other differences). The three other matter distributions, solid sphere, Gaussian and exponential, are in between, and are all compatible with the data.

Within the model, the total multiplicity distribution can be separated into the contribution from (double-) diffractive events, events with one interaction, events with two interactions, and so on, Fig. 13. While 45% of all events contain one interaction, the low-multiplicity tail is dominated by double-diffractive events and the high-multiplicity one by events with several interactions. The average charged multiplicity increases with the number of interactions, Fig. 14, but not proportionally: each additional interaction gives a smaller contribution than the preceding one. This is partly because of energy-momentum-conservation effects, and partly because the additional “messing up” when new string pieces are added has less effect when many strings already are present. The same phenomenon is displayed in Fig. 15, here as a function of the “enhancement factor”  $f(b)$ , i.e., for increasingly central collisions.

The multiplicity distributions for the 200- and 900-GeV UA5 data have not been published, but the moments have,<sup>41</sup> and a comparison with these is presented in Table I. The  $\langle n_{ch} \rangle$  value was brought in reasonable agreement with the data, at each energy separately, by a variation of the  $p_{T0}$  scale. The moments thus obtained are in reasonable agreement with the data.

### B. Energy dependence

Extrapolating to higher energies, the evolution of average charged multiplicity with energy is shown in Fig. 16.

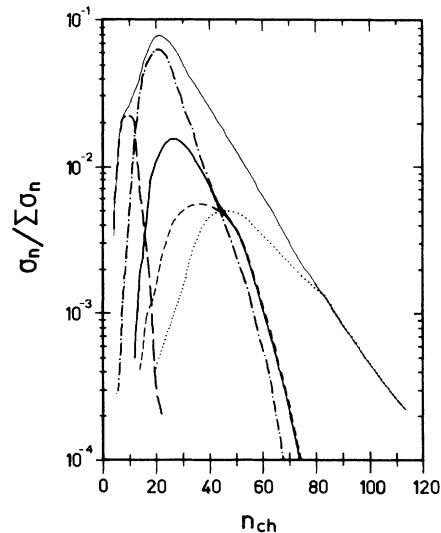


FIG. 13. Separation of multiplicity distribution at 540 GeV by number of interactions in event for double-Gaussian matter distribution. Long dashes, double diffractive; dashed-dotted one interaction; thick solid line, two interactions; dashed line, three interactions; dotted line, four or more interactions; thin solid line, sum of everything.

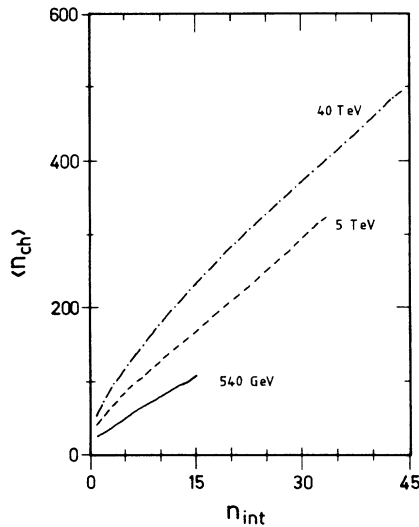


FIG. 14. Average charged multiplicity as a function of the number of interactions. Solid line at 540 GeV, dashed line at 5 TeV, dashed-dotted line at 40 TeV.

The results do depend on the choice of  $p_{T0}$  value, but not crucially so. In addition, the assumptions about flavors and string drawing between scattered partons can be varied to give an even wider band of possible  $\langle n_{ch} \rangle$  at higher energies. The dependence of  $\langle n_{ch} \rangle$  on the number of interactions in the event is shown also for higher energies in Fig. 14, and the dependence on the “enhancement factor”  $f(b)$  is shown in Fig. 15.

The multiplicity distributions themselves are shown in Fig. 17, for 1.6-, 5-, 15-, and 40-TeV c.m. energies, to exemplify the typical shape predicted. The differences that come from the choice of matter distribution are illustrated at 40 TeV in Fig. 18. Contrary to results at  $S\bar{p}\bar{p}S$ , the dependence on this choice is now appreciable. Thus the distributions for a solid sphere, a Gaussian or an exponential all are narrower than for the 540-GeV data, while the double Gaussian produces a much broader shape.

It is interesting to take the ratio  $D/\langle n \rangle$ , the dispersion over the mean, as a measure of the width, and study how the energy variation changes when pieces of physics are added on, Fig. 19. If hadronic events only consisted of one string, spanned between the two outgoing hadron remnants, the multiplicity distribution would be essentially Poissonian, and  $D/\langle n \rangle$  would decrease monotonically

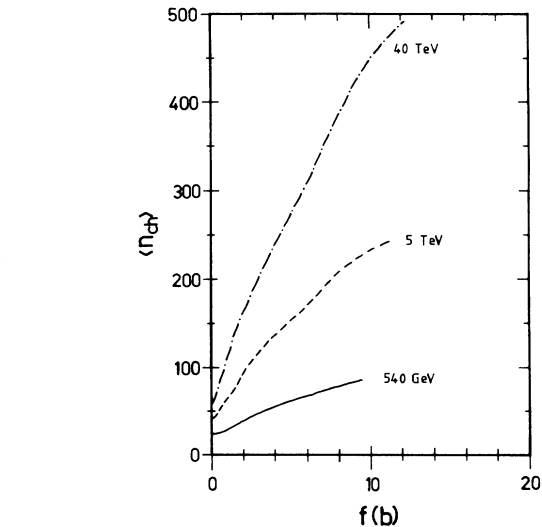


FIG. 15. Average charged multiplicity as a function of the “enhancement factor”  $f(b)$ . Notation as in Fig. 14.

with increasing energy. A minimal model for low- $p_T$  events should probably be based on a two-string model, however. Then the sharing of beam remnant energy would lead to varying invariant masses for the two string pieces, a variation which is enough to understand why  $D/\langle n \rangle$  does not decrease in the fixed-target energy range. (The higher  $D/\langle n \rangle$  value for the one-string model at low energies is due to a lower average multiplicity than in the two-string model or in the data, and the dispersion itself is everywhere smaller with one than with two strings.) At CERN ISR energies, this variation would not suffice, but here hard interactions (including associated initial- and final-state radiation) start to play a role. The effect of having just one interaction is not large, however, and it is only when a varying number of interactions is included that a reasonable description is obtained at  $S\bar{p}\bar{p}S$  energies. If no variation in impact parameter is included, the distribution in number of interactions is again Poissonian, and thus with a relative width that decreases as the average number increases. In fact, the scaled multiplicity distribution would reach its maximum width already at around 1 TeV, in contradiction with the trend of the UA5 data. It is therefore necessary to introduce the variable-impact-parameter picture. The distribution in impact parameter  $b$ , and hence enhancement factor  $f$ , is not governed by Pois-

TABLE I. Moments of the multiplicity distribution at 200, 540, and 900 GeV, UA5 data (Ref. 41) compared with model results.

	200 GeV		540 GeV		900 GeV	
	UA5	Model	UA5	Model	UA5	Model
$\langle n \rangle$	$21.4 \pm 0.8$	21.0	$29.1 \pm 0.9$	28.8	$34.6 \pm 1.2$	34.7
$D$	$10.9 \pm 0.4$	9.9	$16.3 \pm 0.4$	15.8	$20.2 \pm 0.6$	20.5
$\langle n \rangle/D$	$1.96 \pm 0.09$	2.11	$1.79 \pm 0.06$	1.82	$1.72 \pm 0.07$	1.69
$C_2$	$1.26 \pm 0.03$	1.22	$1.31 \pm 0.03$	1.30	$1.34 \pm 0.03$	1.35
$C_3$	$1.91 \pm 0.12$	1.80	$2.12 \pm 0.11$	2.18	$2.22 \pm 0.13$	2.40
$C_4$	$3.3 \pm 0.3$	3.2	$4.1 \pm 0.3$	4.6	$4.3 \pm 0.4$	5.4

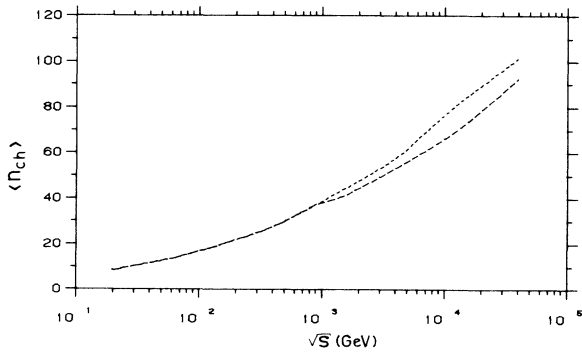


FIG. 16. Average charged multiplicity for nondiffractive events as a function of c.m. energy. Dotted line, assuming that  $p_{T0}=2.0$  is constant above 540 GeV; dashed line, using the logarithmic extrapolation of Eq. (38), cf. Fig. 8.

sonian statistics. Specifically, if the mean number of interactions per event increases with energy, then so does the width of the  $f$  distribution. It is only this step that ensures a nonshrinking multiplicity distribution at higher energies. (The funny bump in  $D/\langle n \rangle$  that appears at around 50 GeV is strongly related to the assumptions about the string drawing for the hardest interaction, Secs. IV D and IV E, and should not be taken too seriously.) Finally, the inclusion of double-diffractive events is a separate issue in our scenario, but one that is needed to understand the low-multiplicity region. It also contributes to the  $D/\langle n \rangle$  ratio measured by experiments.

In our model there is nothing natural about the approximate Koba-Nielsen-Olesen (KNO) scaling<sup>42</sup> observed at lower energies: with the exception of the variable impact parameters, each piece of physics by itself would asymptotically give a shrinking distribution. There is therefore no support for the validity of “two-component”

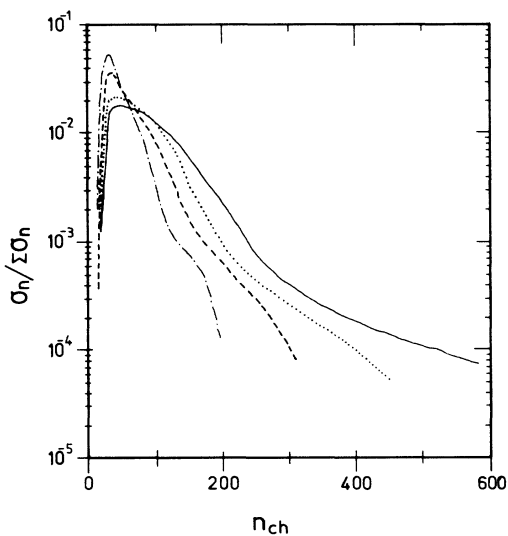


FIG. 17. Predicted multiplicity distributions for higher energies, taking  $p_{T0}=2.0$  GeV and assuming a double-Gaussian matter distribution. Dashed-dotted line, at 1.6 TeV; dashed line, at 5 TeV; dotted line, at 15 TeV; and solid line, at 40 TeV.

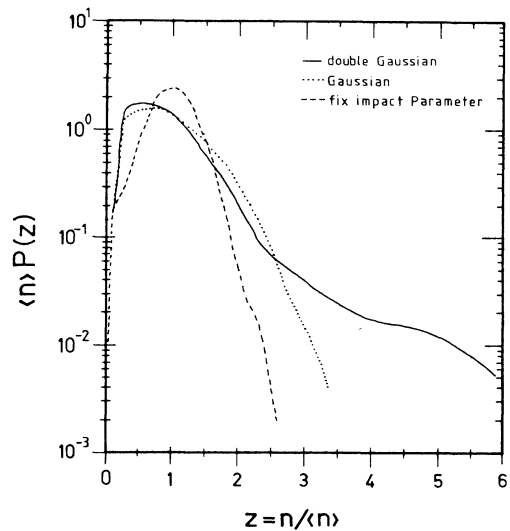


FIG. 18. Scaled multiplicity distribution [KNO plot (Ref. 42)] at 40 TeV. Dashed line, with fix impact parameter ( $\bar{O}_0$ ); dotted line, with Gaussian; and solid line, with double-Gaussian matter distribution.

scenarios,<sup>43</sup> in which minijet events with a higher  $\langle n_{ch} \rangle$  are added on to an immutable low- $p_T$  event KNO distribution.

The DTU-type models<sup>8-11</sup> provide an explanation for the shape of the multiplicity distribution similar to ours. In addition, a number of theoretical models exist in which a simple underlying principle is sought (a few of these are found in Ref. 44). Such models, which often lead to negative-binomial-type multiplicity distributions, are very successful in explaining multiplicity phenomena. There is also an economy of parameters which contrasts markedly

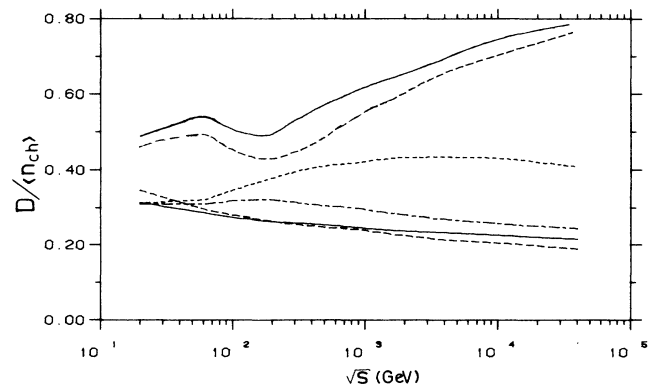


FIG. 19. Ratio  $D/\langle n \rangle$ , i.e., the dispersion over the mean value for the charged-multiplicity distribution, as a function of the c.m. energy, shown as different pieces of physics are successively added on. Lower dashed line, a one-string scenario; lower solid line, simple two-string model; dashed-dotted line, including a hard interaction with initial- and final-state radiation; dotted line, with multiple interactions in the impact-parameter-independent scenario; upper dashed line, with variable impact parameters; and upper solid line, including double-diffractive events.

to the complex scenario outlined in this paper. However, it remains to be seen if the present simplicity can be maintained when these models are extended to cover all particle-production phenomena at hadron colliders, as our model in principle attempts to do.

### C. Multiplicity in pseudorapidity bins

The inclusive pseudorapidity distribution at 200, 540, and 900 GeV is compared with UA5 data<sup>45</sup> in Fig. 20. In fact, the  $p_{T0}$  scales determined from the average total multiplicity had to be lowered by roughly 0.1 GeV in order to achieve the agreement observed; without it the curves would have been below the data almost everywhere. The change corresponds to an increase in the total charged multiplicity at 540 GeV roughly from 29 to 31. It is possible that this comes from differences between our model and the UA5 extrapolations in the region  $|\eta| > 5$ . Note that the dip at  $\eta=0$  is entirely kinematical: had true rapidity been used instead, there would have been no dip. The pseudorapidity distribution for different multiplicity bins is displayed in Fig. 21. Generally, the agreement is satisfactory, but in the low-multiplicity bins we predict a much deeper central dip than observed experimentally. This probably indicates that our diffractive model is not entirely satisfactory. One possibility would be to introduce a component of central diffraction at the expense of double diffraction. Here experimental studies could be of help: are the particles in a given low-multiplicity event still fairly evenly distributed in  $\eta$ , or are they concentrated in a smaller region, the position of which varies from event to event?

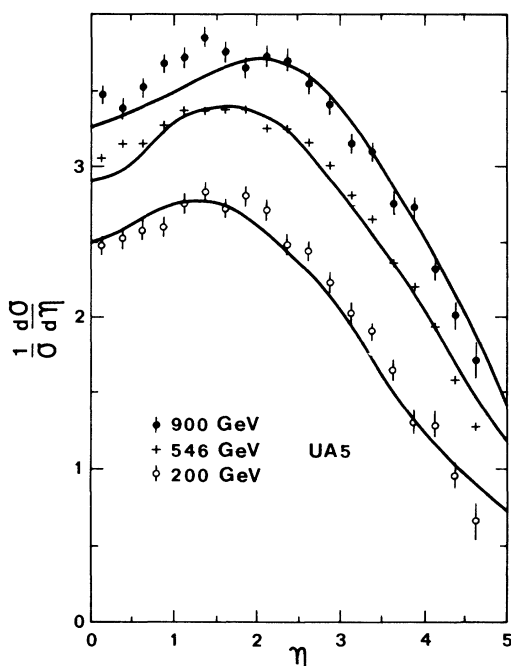


FIG. 20. Charged-particle pseudorapidity distribution at 200, 540, and 900 GeV, from bottom to top. Data points from UA5 (Ref. 45).

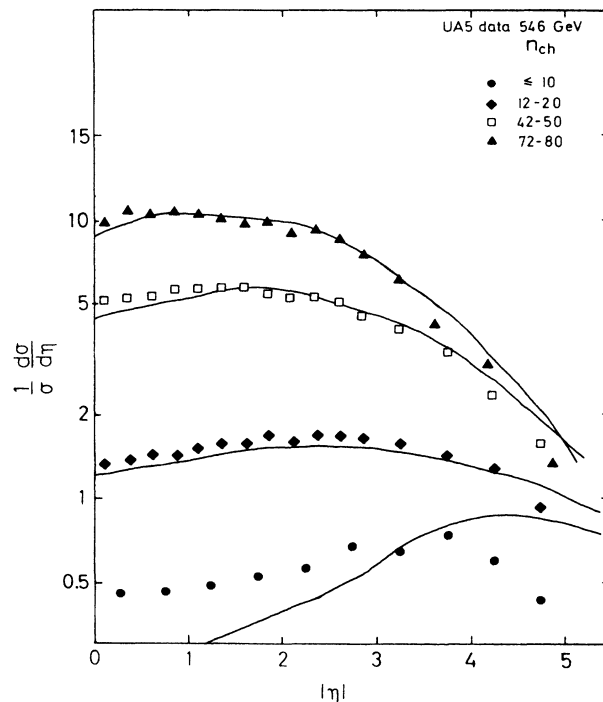


FIG. 21. Charged-particle pseudorapidity distribution at 540 GeV for different bins in total charged multiplicity. From bottom to top for  $n_{ch} \leq 10$ , 12–20, 42–50, and 72–80. Data points from UA5 (Ref. 46).

The comparison with scaled multiplicity distributions in rapidity bins, Fig. 22, shows fair agreement with the UA5 data,<sup>47</sup> but with a tendency to overestimate fluctuations.

Forward-backward multiplicity correlations are again shown in Fig. 23, compared with the UA5 results. It now seems we have somewhat stronger correlations than the data, but it is not incompatible. To some extent, the

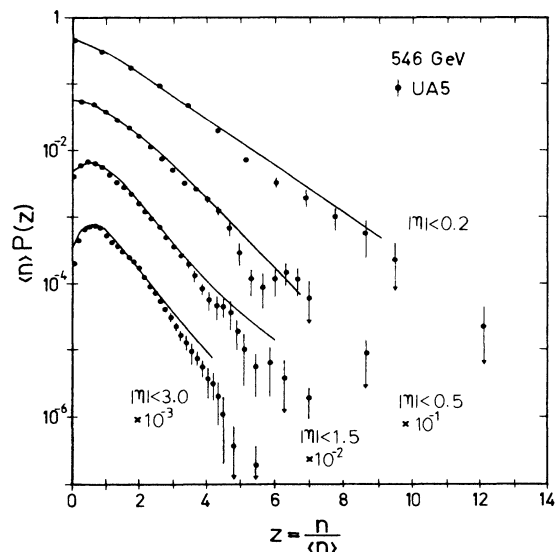


FIG. 22. Scaled multiplicity distributions in pseudorapidity bins, model compared with UA5 data at 540 GeV (Ref. 47).

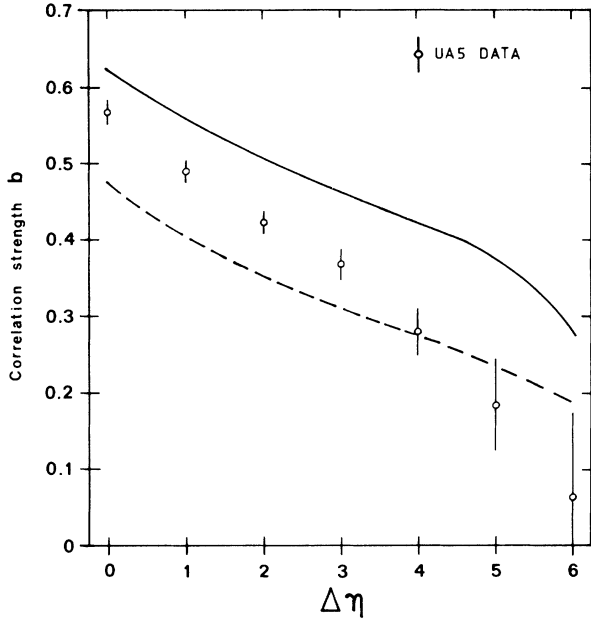


FIG. 23. Forward-backward multiplicity correlations at 540 GeV, UA5 results (Ref. 33) vs multiple-interaction model: solid line, double-Gaussian matter distribution; dashed line, with fix impact parameter ( $\bar{O}_0$ ).

amount of fluctuations and correlations could be “fine-tuned” by a variation of the details of the string drawing, Sec. IV E.

## VI. TRANSVERSE-MOMENTUM PROPERTIES AND JETS

The multiplicity distribution is mainly influenced by longitudinal fragmentation properties. For the transverse-momentum properties, contributions are obtained from the fragmentation of simple strings, and from high- $p_T$  jet production with associated initial- and final-state radiation. These add no new degrees of freedom, but are completely specified by the properties of the model and by our knowledge of  $e^+e^-$  annihilation phenomenology. The only nontrivial input given was to use  $\alpha_s(0.075p_T^2)$  for the hard interaction; an effective  $K$  factor  $\approx 1.5$  or a  $\Lambda \approx 0.7$  GeV (rather than the 0.2 GeV used) would have done as well. It is therefore here that the model can be checked.

Since the comparisons presented elsewhere are made without reference to the particle species involved, Fig. 24

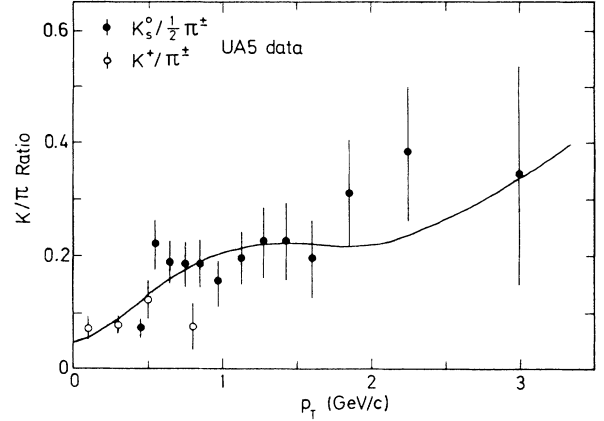


FIG. 24. The  $K/\pi$  ratio as a function of transverse momentum, UA5 data points (Ref. 48), and model results.

serves as a reminder that the model actually also contains predictions for the flavor composition.

### A. Minijets

The UA1 minijet studies contain a wealth of information.<sup>49–51</sup> Unfortunately it is difficult to make a precise comparison with the experimental results without a detailed knowledge of the UA1 detector. All results quoted in the following should therefore be understood to refer to a strongly simplified model of the UA1 detector and UA1 minijet reconstruction procedure, as follows.<sup>4</sup> A detector is assumed to stretch between  $-2.5$  and  $+2.5$  in pseudorapidity, evenly divided into 25 layers of cells, with each layer consisting of 24 cells covering the full azimuth. The transverse energy  $E_T$  (for massive particles equated with the transverse mass) deposited in each cell is summed. A Gaussian smearing of width  $0.5E_T^{1/2}$  is imposed cell by cell, cut off so that the smeared  $E_T$  is never smaller than zero or larger than 4 times the true value. All bins with  $E_T > 1.5$  GeV are taken as possible initiators of jets, and are tried in falling  $E_T$  sequence, to check whether the total  $E_T$  summed over cells within  $\Delta R = [(\Delta\eta)^2 + (\Delta\phi)^2]^{1/2} \leq 1$  exceeds 5 GeV. If so, these cells together define one jet, with position given by the  $E_T$ -weighted center, and are removed from further consideration. Jets which have  $|\eta| > 1.5$  or  $60^\circ < |\phi| < 120^\circ$  are rejected.

With these constraints, the minijet rate and some simple properties in the no-jet and jet samples are shown in Table II. The number of charged particles and their

TABLE II. Minijet phenomenology, comparison between UA1 data (Ref. 49) and model results. Quoted UA1 errors are statistical only.  $\langle n_{\text{ch}} \rangle$  and  $\langle p_T \rangle$  are evaluated for the region  $|\eta| < 2.5$ .

	200 GeV		900 GeV	
	UA1	Model	UA1	Model
Jet event fraction (%)	5.9	5.7	17.2	15.0
$\langle n_{\text{ch}} \rangle_{\text{no jet}}$	$13.81 \pm 0.07$	11.9	$15.93 \pm 0.07$	14.4
$\langle n_{\text{ch}} \rangle_{\text{jet}}$	$26.49 \pm 0.23$	27.9	$32.89 \pm 0.13$	34.2
$\langle p_T \rangle_{\text{no jet}}$ (GeV)	$0.382 \pm 0.005$	0.385	$0.411 \pm 0.005$	0.400
$\langle p_T \rangle_{\text{jet}}$ (GeV)	$0.474 \pm 0.007$	0.453	$0.516 \pm 0.006$	0.496

mean transverse momentum are for particles with  $|\eta| < 2.5$ ; so is the  $\sum E_T$  of all particles. The general agreement is good, but there seems to be a tendency in the model to have too large a split in charged multiplicity between the no-jet and the jet samples. A part of that discrepancy (but not all) is related to an overestimation in the model of the fraction of events with very low multiplicity in  $|\eta| < 2.5$ , and may come from an imperfect simulation of UA1 triggering conditions.

### B. Evidence for multiple interactions

The probability that multiple interactions should give rise to two or more pairs of high- $p_T$  jets is small, in particular when compared with the probability to produce high- $p_T$  jets by a single hard interaction with associated initial- and final-state radiation. It is therefore in the region of relatively small  $p_T$  that effects of multiple interactions are expected to influence the multijet rate. This can be studied by comparing the rate of 1-jet, 2-jet, 3-jet, and 4-jet events in the UA1 minijet analysis. In fact, most events contain only one jet: although jets should be produced in pairs (neglecting radiation), there are many reasons why only one is observed. Jets are only searched for in some angular regions; a bona fide jet is not found if there is no initiator cell with  $E_T > 1.5$  GeV; or a jet may fall below the  $\sum E_T$  requirement while its partner does not, by calorimetric fluctuations or fluctuations in the beam jet background.

A steady decrease in rate as the minijet number is increased is therefore to be expected. The decrease in the data<sup>51</sup> is not as marked as in models without multiple interactions, however (see Table III). Also models with multiple interactions, but without impact-parameter dependence or with a simple Gaussian matter distribution, fail to account for the data. A general agreement is obtained with the double Gaussian matter distribution. In principle, the comparison between data and models is marred by uncertainties in the simulation of the UA1 detector. The absolute rate of jet production could also be changed by variations in the  $K$  factor. These two

effects would tend to compensate each other, so that the relative pattern should be preserved given, e.g., that the 1-jet rate is fixed by data. The case for multiple interactions in the UA1 event sample is therefore strong.

A major uncertainty in the minijet analysis is provided by the calorimetric fluctuations: since the  $E_T$  spectrum is rapidly falling, one gains more minijets by upwards fluctuations than one loses by downwards ones. At 630 GeV, the average number of minijets per event would have been 0.112 without fluctuations, but becomes 0.190 with. A helpful crosscheck would be to redo the minijet analysis using only charged particles. One could then reduce the jet initiator minimum  $E_T$  to 1 GeV and the minijet  $E_T$  threshold to 3 GeV. Assuming that the solid angle covered remains the same, we then obtain almost the same minijet rate as with the ‘‘smeared’’ calorimeter. Also the variation in number of jets and in separation between no-jet and jet samples is preserved.

In the future, it would be interesting to study event properties not only for jet and no-jet events, but also the evolution of  $\langle n_{ch} \rangle$ ,  $\langle p_T \rangle$ , etc., as a function of the number of minijets. This should preferentially also be done for smaller jet opening angles, i.e., smaller  $\Delta R$ .

As noted in the Introduction, evidence for multiple interactions has already been presented by the AFS Collaboration.<sup>14</sup> The AFS Collaboration jets are of about the same  $\sum E_T$  but, because of the smaller c.m. energy (63 GeV), of considerably higher  $x_T$ . Therefore the definition of correlated structure functions is more important. Using a simple recipe similar to the one in this paper, the observed rate of double parton scattering is about a factor 6 higher than expected from Poissonian statistics with no impact-parameter dependence.<sup>14</sup> For the double-Gaussian matter distribution the average enhancement factor  $\langle f(b) \rangle$  in the AFS Collaboration events should be  $\approx 3.7$ , while a simple Gaussian would give only  $\approx 1.7$  (the related  $f_c$  are 0.92 and 0.89, respectively, and do not change the picture). The general trend of the UA1 and the AFS Collaboration data is therefore the same: not only is there evidence for multiple interactions, but at a rate that would suggest regions of denser matter inside the colliding hadrons.

TABLE III. Jet rate and other properties of jet and no jet events at 630 GeV, UA1 data (Refs. 51 and 49), and different models.  $\langle n_{ch} \rangle$ ,  $\langle p_T \rangle$ , and  $\langle \sum E_T \rangle$  are evaluated for the region  $|\eta| < 2.5$ .

	UA1	No multiple interactions	Impact-parameter independent	Simple Gaussian	Double Gaussian
$\geq 1$ jet fraction (%)	14.8	17.0	14.3	13.7	12.6
1 jet fraction (%)	9.96	14.30	11.51	10.79	8.88
2 jet fraction (%)	3.45	2.45	2.45	2.70	2.67
3 jet fraction (%)	1.12	0.22	0.32	0.19	0.74
4 jet fraction (%)	0.22	0.01	0.04	0.05	0.25
5 jet fraction (%)	0.05	0.00	0.00	0.01	0.07
$\langle n_{ch} \rangle_{no\ jet}$	15.06	14.3	11.9	13.5	12.9
$\langle n_{ch} \rangle_{jet}$	32.21	23.7	26.6	30.9	34.2
$\langle p_T \rangle_{no\ jet}$ (GeV)	0.407	0.415	0.398	0.395	0.392
$\langle p_T \rangle_{jet}$ (GeV)	0.502	0.508	0.515	0.473	0.471
$\langle \sum E_T \rangle_{no\ jet}$ (GeV)		13.5	11.0	12.4	12.5
$\langle \sum E_T \rangle_{jet}$ (GeV)		26.2	29.3	32.1	38.2

### C. Correlation between multiplicity and transverse momentum

The KNO multiplicity distributions for the jet and no-jet event samples separately are shown in Fig. 25. One should remember that the seemingly narrow distribution in the jet case is an artifact of using scaled multiplicity; in actual fact the jet event sample at 900 GeV has a width of 17.3 units compared with 8.9 for the no-jet one. In our model, KNO scaling does not hold either for the jet or the no-jet samples, except as an approximation over some limited energy range.

The average transverse momentum of charged particles (with  $|\eta| < 2.5$ ) has also been studied as a function of the charged multiplicity. Results for 200 GeV are shown in Fig. 26; the corresponding figure for 900 GeV is to be found in Ref. 2. The no-jet data are reasonably well reproduced, while agreement is less good for the jet case. At low multiplicities we believe the results to be very sensitive to the details of the minijet trigger, i.e., how often

fluctuations in the calorimeter leads to the reconstruction of “false” minijets. The region of high multiplicities is one of the places where the details of the string drawing does matter, as follows. If the flavor assignment of scattered partons and the string drawing between them are chosen so as to minimize the number of particles produced, then, for a given observed multiplicity, it is necessary to have more interactions (i.e., a smaller  $p_{T0}$ ). With the summed  $p_T$  of scattered partons being large, this is partly inherited by the particles produced. Correspondingly, a maximization of particle production implies the need for fewer interactions and therefore less parton  $p_T$  to be shared. The results at 900 GeV are shown in Fig. 27 for the three extreme scenarios implemented in the program: only  $q\bar{q}$  scatterings, only  $gg$  scatterings with “maximal” string length, and only  $gg$  scatterings with “minimal” string length. In order to obtain the same average multiplicity in the three cases, the  $p_{T0}$  values had to be slightly retuned.

The increase of  $\langle p_T \rangle$  with  $n_{ch}$  is a high-energy phenomenon, and at lower c.m. energies the opposite behavior may be observed. This is not unnatural, since multiplicity fluctuations here come less often from a varying number of interactions and more from the fragmentation and decay components. In Fig. 28 one such comparison is presented, with Split Field Magnet (SFM) data at 63 and 31 GeV (Ref. 52). We do not understand the change in the level of  $\langle p_T \rangle$  values between the 31- and 63-GeV data, but the  $n_{ch}$  dependence is consistent with model results. On the other hand, the  $\langle p_T \rangle$  dependence on  $n_{ch}$  will become even more pronounced as the energy is increased, Fig. 29. [Note that the behavior at small

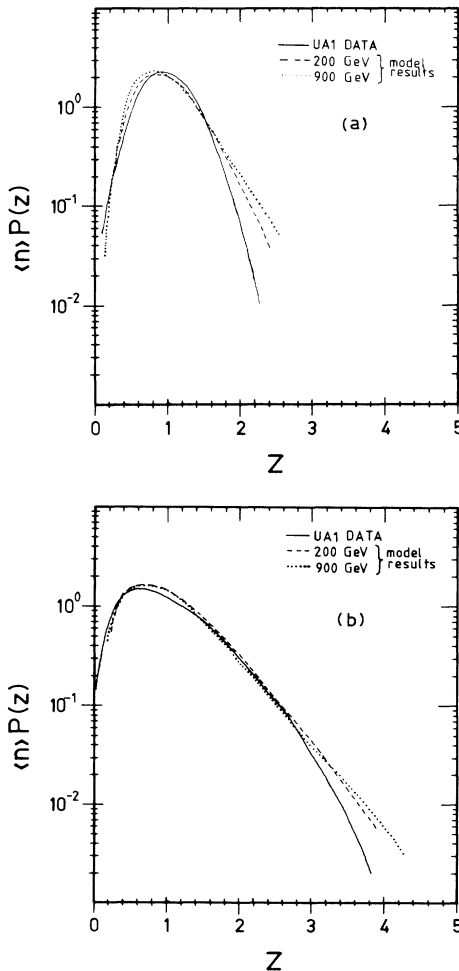


FIG. 25. Scaled multiplicity plots for (a) minijet events and (b) no-jet events. Solid line shows average UA1 data in the range 200–900 GeV (Ref. 49); dashed line is model results at 200 GeV; dotted line, at 900 GeV.

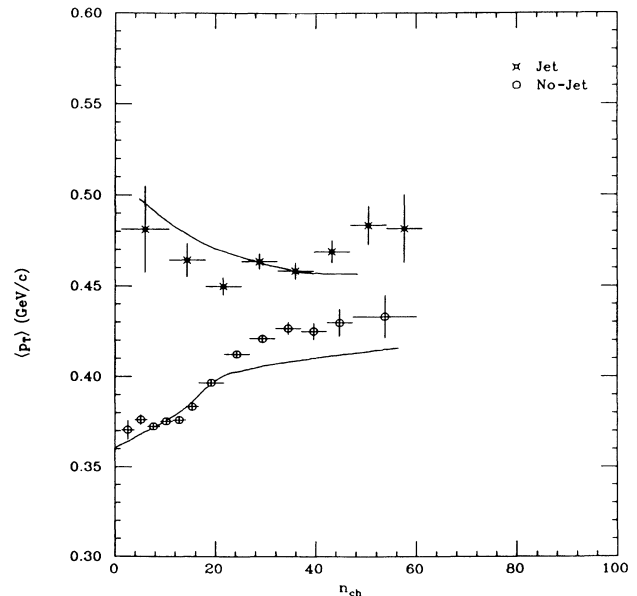


FIG. 26. Average transverse momentum of charged particles in  $|\eta| < 2.5$  as a function of the multiplicity, for jet and no-jet samples separately. UA1 data points at 200 GeV (Ref. 49) compared with model results.

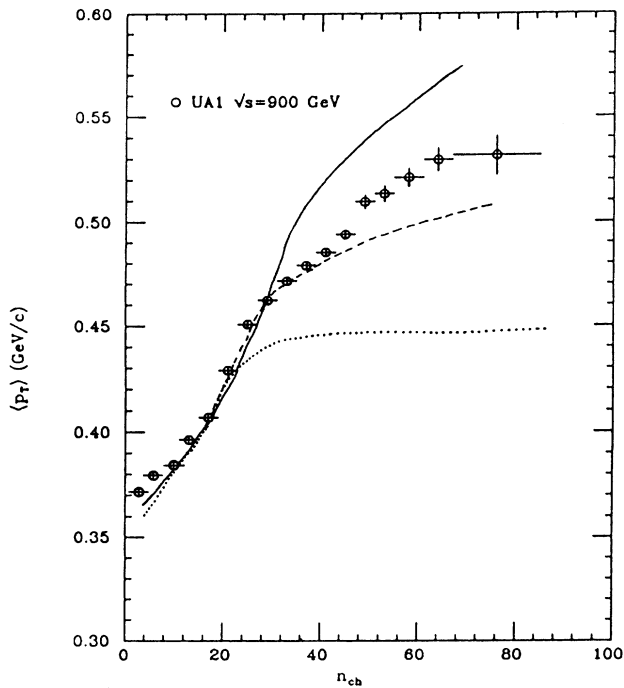


FIG. 27. Average transverse momentum of charged particles in  $|\eta| < 2.5$  as a function of the multiplicity. UA1 data points (Ref. 49) at 900 GeV compared with the model for different assumptions about the nature of the subsequent (nonhardest) interactions. Dashed line, assuming  $q\bar{q}$  scatterings only; dotted line, gg scatterings with “maximal” string length; solid line gg scatterings with “minimal” string length.

multiplicities is affected by the noninclusion of (double-) diffractive events.] The range of populated  $n_{ch}$  values is obviously increasing, and so is the  $\langle n_{ch} \rangle$ , so there is a steady increase with energy of the  $\langle p_T \rangle$  of all charged particles, Fig. 30. The trend is enhanced if only central particles,  $|\eta| < 2$ , are included.

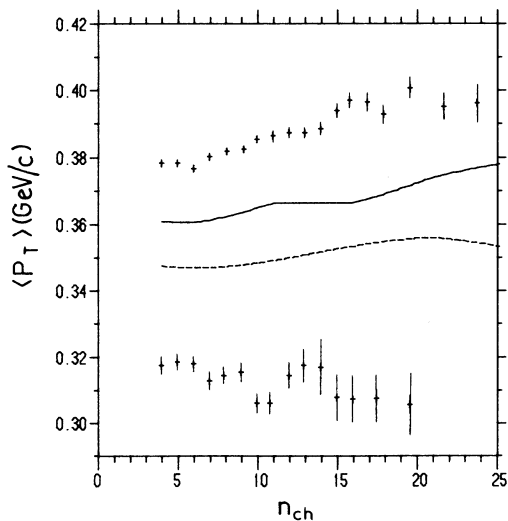


FIG. 28. Average transverse momentum of charged particles in  $|\eta| < 2$  as a function of the multiplicity, SFM data points at 63 and 31 GeV (Ref. 52) vs model curves; solid line, at 63 GeV; and dashed line, at 31 GeV.

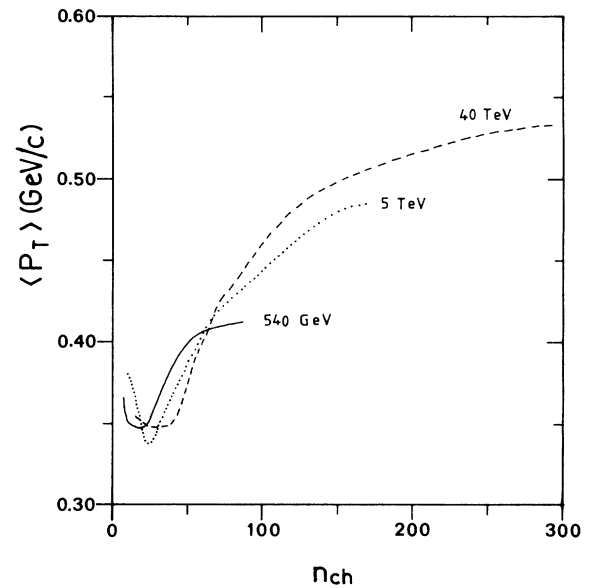


FIG. 29. Average transverse momentum of charged particles in  $|\eta| < 2.5$  as a function of the multiplicity, solid curve, at 540 GeV; dotted curve, at 5 TeV; and dashed curve at 40 TeV. Only nondiffractive events are included.

#### D. Jet profiles

One of the earliest discoveries of jet studies at the  $S\bar{p}\bar{p}S$  was the “pedestal effect,”<sup>35</sup> i.e., that events containing a hard jet also have an above-average particle production away from the jet core. Initial-state radiation may account for part of this effect, but not all.<sup>29</sup> Multiple interactions cannot solve the problem as long as all collisions are assumed to be equivalent,<sup>1</sup> but the introduction of variable impact parameters offers a solution, as follows. Since the average number of jets is larger in central collisions than in peripheral ones, the sample of events containing a hard interaction is biased towards central collisions. These events are then likely to contain additional jet activity. We will now proceed to show that our standard multiple-interaction scenario, with a double Gaussian matter distribution, indeed gives a satisfactory agreement with data.

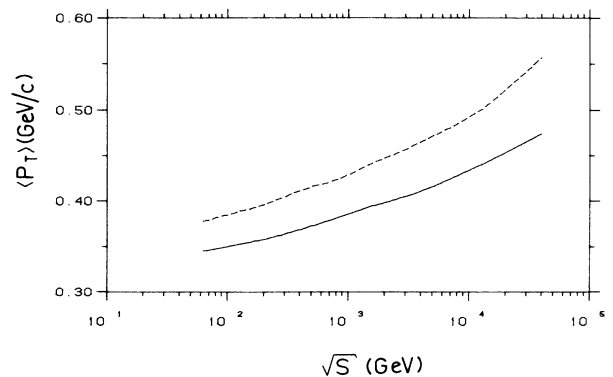


FIG. 30. Average transverse momentum as a function of the c.m. energy, solid line is all charged particles, dashed line is charged particles with  $|\eta| < 2$ .

Jet profiles for 5-, 10-, and 30-GeV jet triggers are compared with UA1 data at 630 GeV (Ref. 50) in Fig. 31. The quantity shown is  $dE_T/d\eta$  as a function of  $\eta - \eta_{\text{jet}}$  in the “same side” region  $|\phi - \phi_{\text{jet}}| < 90^\circ$ . One should emphasize that, for the lower jet energies, the profile of the jet core is significantly broadened by the redefinition of the  $\eta_{\text{jet}}$  to be the  $E_T$ -weighted center rather than the position of the initiator cell.

The average value of the  $dE_T/d\eta$  in the range  $1 \leq |\eta - \eta_{\text{jet}}| \leq 2$  is shown in Fig. 32 as a function of  $E_{T\text{jet}}$ . Note the seeming inconsistency in UA1 data between Fig. 31 and Fig. 32; we choose to trust the latter. The curve has been extended below  $E_{T\text{jet}} = 5$  GeV by forming a jet around any initiator cell with  $E_T \geq 1.5$  GeV. The rise of  $\langle dE_T/d\eta \rangle$  up to  $E_{T\text{jet}} \approx 12$  GeV is due to a shift in the composition of events, from one dominated by fairly peripheral collisions to one strongly biased towards central ones. In the model, there is a limit for how far this biasing can go: once

$$\int_{p_T}^{s^{1/2}/2} \frac{d\sigma}{dp_T'} dp_T' = \sigma_{\text{hard}}(p_T) \ll \sigma_{\text{ND}}, \quad (39)$$

the exponential in Eq. (34) can be neglected. The probability distribution in  $b$  is then given by  $\tilde{O}(b)d^2b$ , independently of the  $p_T$  value. The condition (39) is fulfilled for  $p_T \approx E_{T\text{jet}} \approx 10$  GeV, leading to a plateau above that. There is even a slight drop with energy, due to a change from predominantly gluon-gluon scatterings to predominantly quark-quark ones.<sup>29</sup> By comparison, in a scenario without multiple interactions, there is no natural mechanism for obtaining a significant pedestal effect. Furthermore, whereas the  $E_{T\text{jet}}$  value where a plateau is attained is a stable prediction of the model, the height of that plateau is sensitive to the hadronic matter distribution assumed, Fig. 32. The standard double Gaussian here gives a good description.

At higher energies, the level of the plateau is predicted

to increase successively, but the  $E_{T\text{jet}}$  value where the plateau starts will vary only slowly. In Fig. 33 some jet profiles at 2, 10, and 40 TeV (still using the UA1-inspired jet algorithm; results could well be slightly different with the actual CDF/D0, etc., reconstruction procedures) are shown. Figure 34 contains the predictions for the plateau level  $\langle dE_T/d\eta \rangle(E_{T\text{jet}})$  in  $1 \leq |\eta - \eta_{\text{jet}}| \leq 2$ .

## VII. SUMMARY AND OUTLOOK

In this paper we have tried to present a realistic model for particle production in hadron-hadron collisions. If the measure of success is the degree of simplicity achieved, then ours is a complete failure. From physics considerations, backed by comparisons with data, we have been led to the formulation of a very complex and detailed model. The list of factors that influence the multiplicity distribution (Sec. VB) contains six major points, each of which requires the development of specific models, and each of which has a number of free parameters. Yet, it is very difficult to imagine how any of the six points could be discarded in order to obtain a simpler model. It is therefore likely that a better model would also have to be an even more detailed one.

Considering the complexity and the number of unanswered questions, is it meaningful to trust the model at all? Probably yes, at least up to a point. Many of the components can be independently checked: fragmentation and parton showers in  $e^+e^-$  annihilation, hard parton-parton interactions (whether one per event or more) by jet studies, and so on. In this paper we have presented several successful comparisons with data, and a few not so successful. In particular, the model provides an understanding of the event rate of multiple minijet production and the variation of pedestal level with jet energy, effects which are not easily accommodated in simpler models. The main problem seems to be the understanding of low-

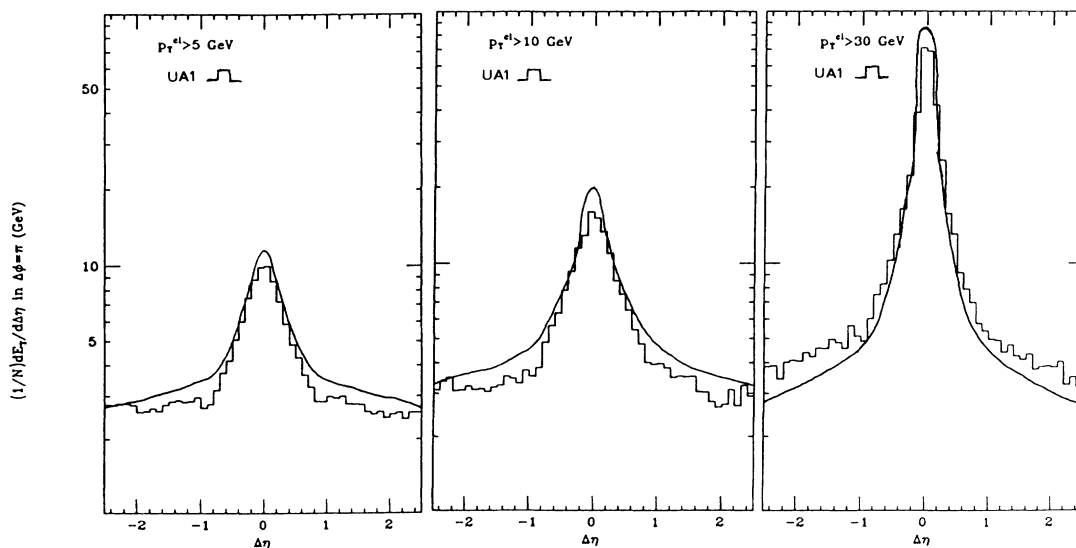


FIG. 31. Jet profiles,  $dE_T/d\eta$  as a function of  $\eta - \eta_{\text{jet}}$ , in the “same side” region  $|\phi - \phi_{\text{jet}}| < 90^\circ$ . Histograms are UA1 data at 630 GeV (Ref. 50) and the curves represent model results. (a)  $E_{T\text{jet}} > 5$  GeV. (b)  $E_{T\text{jet}} > 10$  GeV. (c)  $E_{T\text{jet}} > 30$  GeV.

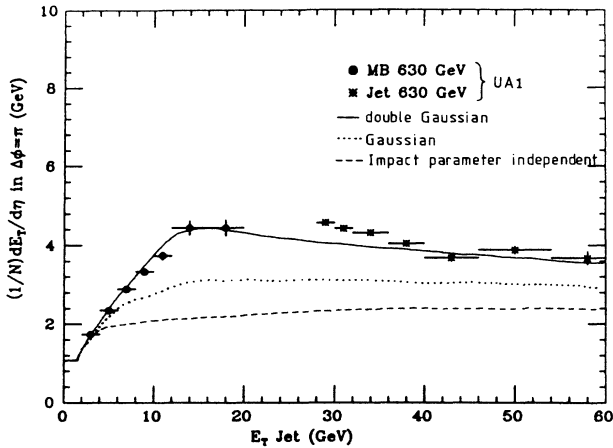


FIG. 32. Average transverse energy  $\langle dE_T/d\eta \rangle$  in  $1 \leq |\eta - \eta_{\text{jet}}| \leq 2$ ,  $|\phi - \phi_{\text{jet}}| < 90^\circ$  as a function of the  $E_{T\text{jet}}$  trigger. Data points UA1 at 630 GeV (Ref. 50), dashed curve represents the impact-parameter-independent model, dotted curve represents Gaussian, and solid curve represents double-Gaussian matter distribution.

multiplicity events, be that double diffractive or whatever. Since the complete model is publicly available in Monte Carlo form,<sup>3,4</sup> further checks could be made in the context of more realistic detector simulations.

In addition, different uncertainties do not necessarily add up the way one might expect. If some detail in the model is varied, generally the  $p_{T0}$  scale has to be retuned somewhat to retain the same average charged multiplicity, and the two changes usually tend to compensate each other. This is one of the reasons why the major uncertainties in string-drawing issues (and in quark-gluon composition of scattered flavors) are not all that important for the overall picture.

It is easy to enumerate aspects where further studies ought to be made, if only one knew how. The model contains none of the quantum-mechanical complexities that must be there, such as interference effects between different semihard interactions. The simultaneous definition of structure functions for several partons inside a hadron is achieved in the most naive fashion possible.

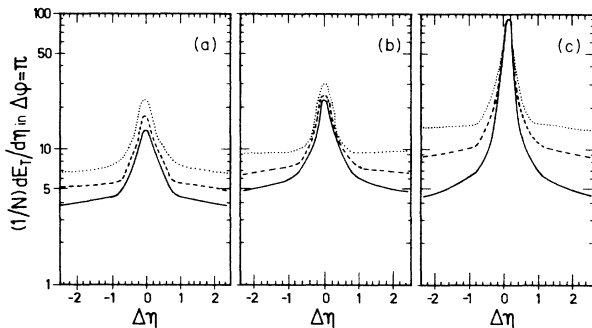


FIG. 33. Jet profiles,  $dE_T/d\eta$  as a function of  $\eta - \eta_{\text{jet}}$ , in the "same side" region  $|\phi - \phi_{\text{jet}}| < 90^\circ$ . Solid line, model results at 2 TeV; dashed line, results at 10 TeV; and dotted line, results at 40 TeV (with UA1-inspired jet algorithm). (a)  $E_{T\text{jet}} > 5$  GeV. (b)  $E_{T\text{jet}} > 10$  GeV. (c)  $E_{T\text{jet}} > 30$  GeV.

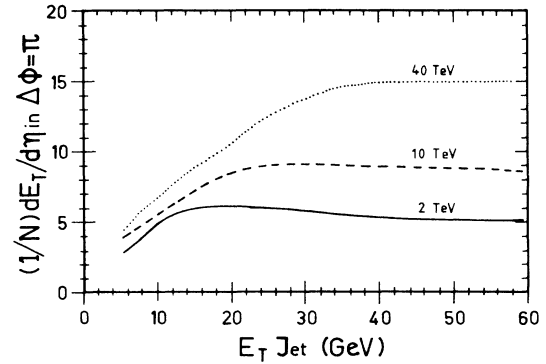


FIG. 34. Average transverse energy  $\langle dE_T/d\eta \rangle$  in  $1 \leq |\eta - \eta_{\text{jet}}| \leq 2$ ,  $|\phi - \phi_{\text{jet}}| < 90^\circ$  as a function of the  $E_{T\text{jet}}$  trigger (UA1-inspired jet algorithm). Solid curve, results at 2 TeV; dashed curve, results at 10 TeV; and dotted curve, results at 40 TeV.

The whole description of a hadronic matter distribution for the colliding hadrons, with the spatial distribution of partons completely decoupled from the momentum distribution, is overly simplistic. The regularization of the perturbative QCD cross section at small  $p_T$  values, although not unreasonable, is certainly arbitrary. A description in terms of independently fragmenting simple color strings may or may not be a good approximation to what is actually happening. The choice of color flow structure is only a first attempt. Multiple interactions could come from one initial parton cascading into many, whereof several scatter against partons in the colliding hadron; this could actually be the reason why we were forced to introduce local concentrations of matter inside the hadrons.

In conclusion, the model presented here offers a description of high- $p_T$  and low- $p_T$  phenomena within one single framework. It may be used as a base on which further developments could be added. The ultimate objective, to provide a description of all particle-production phenomena in hadron collisions, is obviously not yet within reach. Important further tests of the basic ideas will already come with the data from the new Fermilab Tevatron I collider and, on a longer time scale, with the advent of the Superconducting Super Collider and the CERN Large Hadron Collider.

*Note added in proof.* The minijet rates reported in Table III are based on the use of true rapidity, rather than pseudorapidity, in the jet-finding algorithm. This unfortunate programming error gives an overestimation of rates by roughly 30%, but the qualitative picture is not changed. The resulting uncertainty may still be less than that coming from the lack of a complete simulation of the UA1 detector. None of the conclusions reached in this paper are therefore affected.

#### ACKNOWLEDGMENTS

We would like to thank H.-H. Thodberg for stimulating discussions on the AFS jet studies and H.-U. Bengtsson for inspiring collaboration in the development of PYTHIA. One of us (T.S.) would also like to thank C.-E. Wulz for helpful discussions on the UA1 minijet analysis.

- <sup>1</sup>T. Sjöstrand, Fermilab Report No. Pub-85/119-T, 1985 (unpublished).
- <sup>2</sup>T. Sjöstrand and M. van Zijl, Phys. Lett. B **188**, 149 (1987).
- <sup>3</sup>H.-U. Bengtsson and T. Sjöstrand, Comput. Phys. Commun. (to be published).
- <sup>4</sup>T. Sjöstrand, Comput. Phys. Commun. **39**, 347 (1986); T. Sjöstrand and M. Bengtsson, *ibid.* **43**, 367 (1987).
- <sup>5</sup>P. V. Landshoff and J. C. Polkinghorne, Phys. Rev. D **18**, 3344 (1978); C. Goebel, D. M. Scott, and F. Halzen, *ibid.* **22**, 2789 (1980).
- <sup>6</sup>N. Paver and D. Treleani, Nuovo Cimento **70A**, 215 (1982); **73A**, 392 (1983); Phys. Lett. **146B**, 252 (1984); Z. Phys. C **28**, 187 (1985).
- <sup>7</sup>B. Humpert, Phys. Lett. **131B**, 461 (1983); B. Humpert and R. Odorico, *ibid.* **154B**, 211 (1985).
- <sup>8</sup>V. A. Abramovski, O. V. Kancheli, and V. N. Gribov, in *Proceedings of the XVI International Conference on High Energy Physics*, edited by J. D. Jackson, A. Roberts, and R. Donaldson (National Accelerator Laboratory, Batavia, 1972), Vol. 1, p. 389.
- <sup>9</sup>A. Capella and J. Tran Thanh Van, Phys. Lett. **114B**, 450 (1982); Z. Phys. C **18**, 85 (1983); **23**, 165 (1984); A. Capella, A. Staar, and J. Tran Thanh Van, Phys. Rev. D **32**, 2933 (1985).
- <sup>10</sup>P. Aurenche and F. W. Bopp, Phys. Lett. **114B**, 363 (1982); P. Aurenche, F. W. Bopp, and J. Ranft, Z. Phys. C **23**, 67 (1984); **26**, 279 (1984); Phys. Lett. **147B**, 212 (1984).
- <sup>11</sup>K. Fiałkowski and A. Kotanski, Phys. Lett. **107B**, 132 (1981); **115B**, 425 (1982); A. B. Kaidalov, Phys. Lett. **116B**, 459 (1982); A. B. Kaidalov and K. A. Ter Martirosyan, Phys. Lett. **117B**, 247 (1982).
- <sup>12</sup>A. Białas and E. Białas, Acta Phys. Pol. **B5**, 373 (1974), and references therein; T. T. Chou and C. N. Yang, Phys. Rev. D **32**, 1692 (1985); S. Barshay, Z. Phys. C **32**, 513 (1986); W. R. Chen and R. C. Hwa, Phys. Rev. D **36**, 760 (1987).
- <sup>13</sup>T. T. Chou and C. N. Yang, Phys. Rev. **170**, 1591 (1968); Phys. Rev. D **19**, 3268 (1979); C. Bourrely, J. Soffer, and T. T. Wu, Nucl. Phys. **B247**, 15 (1984); P. L'Heureux, B. Margolis, and P. Valin, Phys. Rev. D **32**, 1681 (1985); L. Durand and H. Pi, Phys. Rev. Lett. **58**, 303 (1987).
- <sup>14</sup>AFS Collaboration, T. Åkesson *et al.*, Z. Phys. C **34**, 163 (1987).
- <sup>15</sup>E. Eichten, I. Hinchliffe, K. Lane, and C. Quigg, Rev. Mod. Phys. **56**, 579 (1984); **58**, 1065 (1986).
- <sup>16</sup>R. K. Ellis and J. C. Sexton, Nucl. Phys. **B269**, 445 (1986).
- <sup>17</sup>L. V. Gribov, E. M. Levin, and M. G. Ryskin, Phys. Rep. **100**, 1 (1983).
- <sup>18</sup>A. H. Mueller and J. Qiu, Nucl. Phys. **B268**, 427 (1986).
- <sup>19</sup>J. P. Ralston and D. W. McKay, in *Physics Simulations at High Energy*, edited by V. Barger, T. Gottschalk, and F. Halzen (World Scientific, Singapore, 1987), p. 30.
- <sup>20</sup>J. C. Collin, in *Observable Standard Model Physics at the SSC: Monte Carlo Simulation and Detector Capabilities*, edited by H.-U. Bengtsson, C. Buchanan, T. Gottschalk, A. Soni (World Scientific, Singapore, 1986), p. 15.
- <sup>21</sup>M. M. Block and R. N. Cahn, Rev. Mod. Phys. **57**, 563 (1985); in *Physics Simulations at High Energy* (Ref. 19), p. 89.
- <sup>22</sup>K. Goulianos, Phys. Rep. **101**, 169 (1983).
- <sup>23</sup>J. Kuti and V. F. Weisskopf, Phys. Rev. D **4**, 3418 (1971); H. R. Gerhold, Nuovo Cimento **59A**, 373 (1980).
- <sup>24</sup>A. Capella and J. Tran Thanh Van, Z. Phys. C **10**, 249 (1981).
- <sup>25</sup>A. Capella, U. Sukhatme, C. I. Tan, and J. Tran Thanh Van, Phys. Lett. **81B**, 68 (1979).
- <sup>26</sup>G. Gustafson, Z. Phys. C **15**, 155 (1982); H.-U. Bengtsson, Comput. Phys. Commun. **31**, 323 (1984).
- <sup>27</sup>M. Bengtsson and T. Sjöstrand, Phys. Lett. B **185**, 435 (1987); Nucl. Phys. **B289**, 810 (1987).
- <sup>28</sup>A. H. Mueller, Phys. Lett. **104B**, 161 (1981); B. I. Ermolaev and V. S. Fadin, JETP Lett. **33**, 269 (1981); A. Bassetto, M. Ciafaloni, and G. Marchesini, Phys. Rep. **100**, 201 (1983); G. Marchesini and B. R. Webber, Nucl. Phys. **B238**, 1 (1984).
- <sup>29</sup>T. Sjöstrand, Phys. Lett. **157B**, 321 (1985); M. Bengtsson, T. Sjöstrand, and M. van Zijl, Z. Phys. C **32**, 67 (1986).
- <sup>30</sup>B. Andersson, G. Gustafson, G. Ingelman, and T. Sjöstrand, Phys. Rep. **97**, 33 (1983).
- <sup>31</sup>T. Sjöstrand, Phys. Lett. **142B**, 420 (1984); Nucl. Phys. **B248**, 469 (1984).
- <sup>32</sup>UA5 Collaboration, G. J. Alner *et al.*, Phys. Lett. **138B**, 304 (1984).
- <sup>33</sup>J. Gaudean, Ph.D. thesis, Universiteit Antwerpen, 1984.
- <sup>34</sup>J. G. Rushbrooke, in *Proceedings of  $p\bar{p}$  Options for the Super-collider*, edited by J. A. Pilcher and A. R. White (unpublished), p. 176.
- <sup>35</sup>UA1 Collaboration, G. Arnison *et al.*, Phys. Lett. **132B**, 214 (1983).
- <sup>36</sup>G. E. Brown and M. Rho, Phys. Lett. **82B**, 177 (1979).
- <sup>37</sup>I. Montvay, Phys. Lett. **84B**, 331 (1979).
- <sup>38</sup>S. Fredriksson, M. Jändel, and T. Larsson, Z. Phys. C **19**, 53 (1983).
- <sup>39</sup>A. Breakstone *et al.*, Z. Phys. C **28**, 335 (1985).
- <sup>40</sup>G. Ingelman and P. E. Schlein, Phys. Lett. **152B**, 256 (1985).
- <sup>41</sup>UA5 Collaboration, G. J. Alner *et al.*, Phys. Lett. **167B**, 476 (1986).
- <sup>42</sup>Z. Koba, H. B. Nielsen, and P. Olesen, Nucl. Phys. **B40**, 317 (1972).
- <sup>43</sup>T. V. Gaisser and F. Halzen, Phys. Rev. Lett. **54**, 1754 (1985); G. Panzeri and Y. Srivastava, Phys. Lett. **159B**, 69 (1985); A. D. Martin and C. J. Maxwell, *ibid.* **172B**, 248 (1986).
- <sup>44</sup>P. Carruthers and C. C. Shih, Phys. Lett. **127B**, 242 (1983); C. S. Lam and M. A. Walton, *ibid.* **140B**, 246 (1984); A. Giovanni and L. Van Hove, Z. Phys. C **30**, 391 (1986); B. Durand and I. Sarcevic, Phys. Lett. **172B**, 104 (1986).
- <sup>45</sup>UA5 Collaboration, G. J. Alner *et al.*, Z. Phys. C **33**, 1 (1986).
- <sup>46</sup>UA5 Collaboration, G. J. Alner *et al.*, Nucl. Instrum. Methods (to be published).
- <sup>47</sup>UA5 Collaboration, G. J. Alner *et al.*, Phys. Lett. **160B**, 193 (1985).
- <sup>48</sup>UA5 Collaboration, G. J. Alner *et al.*, Nucl. Phys. **B258**, 505 (1985).
- <sup>49</sup>UA1 Collaboration, F. Ceradini, in *Proceedings of the International Europhysics Conference on High Energy Physics*, Bari, Italy, 1985, edited by L. Nitti and G. Preparata (Laterza, Bari, 1985), p. 363.
- <sup>50</sup>UA1 Collaboration, C. Albajar, in *Physics Simulations at High Energy* (Ref. 19), p. 39; UA1 Collaboration, A. Di Ciaccio, in *Proceedings of the XVII International Symposium on Multiparticle Dynamics*, Seewinkel, Austria, 1986, edited by M. Markytan, W. Majerotto, and J. MacNaughton (World Scientific, Singapore, 1987) p. 679; UA1 Collaboration, F. Lacava, Proceedings of the 6th Topical Workshop on Proton-Antiproton Physics, Aachen, Germany, 1986 (unpublished).
- <sup>51</sup>UA1 Collaboration, C.-E. Wulz, Report No. CERN-EP/87-84, 1987 (unpublished); and private communications.
- <sup>52</sup>A. Breakstone, *et al.*, Phys. Lett. **132B**, 463 (1983).